DESIGN OF A REAL-TIME SCANNING ELECTRICAL MOBILITY SPECTROMETER AND ITS APPLICATION IN STUDY OF NANOPARTICLE AEROSOL GENERATION

A Thesis

by

GAGAN SINGH

Submitted to the Office of Graduate Studies of
Texas A&M University
in partial fulfillment of the requirements for the degree of

MASTER OF SCIENCE

May 2010

Major Subject: Mechanical Engineering

DESIGN OF A REAL-TIME SCANNING ELECTRICAL MOBILITY SPECTROMETER AND ITS APPLICATION IN STUDY OF NANOPARTICLE AEROSOL GENERATION

A Thesis

by

GAGAN SINGH

Submitted to the Office of Graduate Studies of
Texas A&M University
in partial fulfillment of the requirements for the degree of

MASTER OF SCIENCE

Approved by:

Chair of Committee,	Bing Guo
Committee Members,	Renyi Zhang
	Eric Petersen
Head of Department,	Dennis O'Neal

May 2010

Major Subject: Mechanical Engineering

ABSTRACT

Design of a Real-Time Scanning Electrical Mobility Spectrometer and Its Application in Study of Nanoparticle Aerosol Generation. (May 2010)

Gagan Singh, B.S., Texas A&M University

Chair of Advisory Committee: Dr. Bing Guo

A real-time, mobile Scanning Electrical Mobility Spectrometer (SEMS) was designed using a Condensation Particle Counter (CPC) and Differential Mobility Analyzer (DMA) to measure the size distribution of nanoparticles. The SEMS was calibrated using monodisperse Polystyrene Latex (PSL) particles, and was then applied to study the size distribution of TiO_2 nanoparticle aerosols generated by spray drying water suspensions of the nanoparticles. The nanoparticle aerosol size distribution, the effect of surfactant, and the effect of residual solvent droplets were determined.

The SEMS system was designed by integrating the Electrical System, the Fluid Flow System, and the SEMS Software. It was calibrated using aerosolized Polystyrene Latex (PSL) spheres with nominal diameters of 99 nm and 204 nm. TiO_2 nanoparticle aerosols were generated by atomizing water suspensions of TiO_2 nanoparticles using a Collison nebulizer. Size distribution of the TiO_2 aerosol was measured by the SEMS, as well as by TEM. Furthermore, the effect of surfactant, Tween 20 at four different concentrations between 0.01mM and 0.80mM, and stability of aerosol concentration with time were studied. It was hypothesized that residual particles in DI water observed

during the calibration process were a mixture of impurities in water and unevaporated droplets. Solid impurities were captured on TEM grids using a point-to-plane Electrostatic Precipitator (ESP) and analyzed by Energy Dispersive Spectroscopy (EDS) while the contribution of unevaporated liquid droplets to residual particles was confirmed by size distribution measurements of aerosolized DI water in different humidity conditions.

The calibration indicated that the mode diameter was found to be at 92.5nm by TEM and 95.8nm by the SEMS for 99nm nominal diameter particles, a difference of 3.6%. Similarly, the mode diameter for 204nm nominal diameter particles was found to be 194.9nm by TEM and 191nm by SEMS, a difference of 2.0%. Measurements by SEMS for TiO_2 aerosol generated by Collison nebulizer indicated the mode diameters of 3mM, 6mM, and 9mM concentrations of TiO_2 suspension to be 197.5nm, 200.0nm and 195.2nm respectively. On the other hand, the mode diameter was found to be approximately 95nm from TEM analysis of TiO_2 powder. Additionally, concentration of particles generated decreased with time. Dynamic Light Scattering (DLS) measurements indicated agglomeration of particles in the suspension. Furthermore, the emulation of single particle distribution was not possible even after using Tween 20 in concentrations between 0.01mM and 0.80mM. From the study of residual particles in DI water, it was found that residual particles observed during the aerosolization of suspensions of DI water were composed of impurities present in DI water and unevaporated droplets of DI water. Although it was possible to observe solid residual particles on the TEM grid, EDS was not able to determine the chemical composition of these particles.

ACKNOWLEDGEMENTS

I would like to thank my committee chair, Dr. Bing Guo, for his valuable support and guidance throughout the course of this research. I would also like to thank Dr. Eric Petersen and Dr. Renyi Zhang for their recommendations and consideration as committee members.

I am very grateful to Alexei Khalizov for sharing his expertise in the design of SEMS system, Wonjoong Hwan for his help with TEM analysis and Andrew Sharp for sharing his programming knowledge to create the SEMS software.

Finally, I would like to extend my gratitude to my parents for their encouragement and support throughout my time here at Texas A&M University.

TABLE OF CONTENTS

Page

LIST OF FIGURES

Page

Page

LIST OF TABLES

1. INTRODUCTION

Size is perhaps the most fundamental parameter describing an aerosol. Particles in aerosols can be many orders of magnitude, from just a few nanometers to around 100 micrometer (Baron and Willeke 2001). Physical and chemical properties of aerosols depend on their size distribution and thus, it is an essential feature of aerosol study. A number of researchers analyze size distribution of aerosols to reach valuable conclusions. Size distribution measurement is an important analytical tool in a number of fields such as atmospheric sciences, combustion studies, flame synthesis of particles and in the area of health and safety. For example, analysis of soot nanoparticles is done by characterizing combustion soot by studying its size distribution (Zhao et al. 2003). Another example is the measurement of modes and geometric means of particles near a major highway to determine exposure to ultrafine particles (Zhu et al. 2002).

Various tools can be used to determine size distribution of aerosols. These include the Electrical Aerosol Analyzer (EAA), Scanning Electrical Mobility Spectrometer (SEMS), Optical Particle Counters, Cascade Impactors and Aerodynamic Particle Sizers (APS). Among these, the SEMS is perhaps the most widely used instrument for size distribution measurements. A differential mobility analyzer (DMA) classifies particles into a narrow range of mobility which are then counted by a condensation particle counter (CPC). The first differential mobility analyzer was developed by Erikson (1921) for understanding the evolution of mobility of small ions.

This thesis follows the style of *Aerosol Science and Technology*.

Even though this instrument could provide differential measurements of ion mobility with high resolution, lack of a suitable detector limited its use. Development of continuous flow condensation particle counter by Bricard and coworkers provided the required sensitivity and time response for particle size distribution measurements (Flagan 1998). The SEMS is commercially available as the Scanning Mobility Particle Sizer (SMPS) system and is offered by TSI, Inc.

Major advantages of the SEMS system include its ease of transportation, low power consumption, and high resolution in measurement of particles. The SEMS also has an important advantage over the stepping mode of operation. Many systems such as smog chambers, combustion sources and industrial processes change composition rapidly. The scanning mode is appropriate for determining particle size distribution in these cases as significant noise is observed in the signals in stepping mode (Wang and Flagan 1990). Typical time required for completing a particle size distribution measurement in stepping mode varies from 10 minutes to an hour or more. Concentrations for over 100 mobilities can be measured using the scanning mode in 20 to 30s as found by Wang and Flagan. In this paper, the design and calibration of a SEMS system is described. This not only offers a cheaper alternative to the otherwise expensive commercially available systems but also can be customized to the needs of the researcher. Finally, the SEMS system has been applied to study the generation of Titanium dioxide nanoparticles using a Collison nebulizer and residual particles in the aerosolized De-ionized water. These studies are also described in the thesis.

2. SCANNING ELECTRICAL MOBILITY SPECTROMETER-DESIGN AND CALIBRATION

2.1 General Operating Principles

2.1.1 Theory

The Scanning Electrical Mobility Spectrometer (SEMS) operates by classifying particles based on electrical mobility and counting the particles using a detector. In the system, the aerosol first passes through a bipolar charger which creates negative and positive charges on particles and reaches a Fuchs' equilibrium charge distribution. The aerosol particles then pass through a Differential Mobility Analyzer (DMA) in which they are separated according to their electrical mobility. The SEMS operating principle can be explained with the help of the DMA schematic in Figure 1.

The DMA consists of the inner and outer electrodes in the form of concentric cylinders. A high voltage is applied to the inner electrode which attracts particles of the opposite charge. The outer electrode is kept at ground potential and particles having the same polarity of charge as the inner electrode are deposited on the wall. Neutral particles exit along with excess air. HEPA-filtered sheath air is introduced in the DMA and flows in the annular space between the electrodes. The flows for both the sheath air and aerosol flow are controlled upstream of the DMA. Particles in a narrow range of

mobility exit through the sample exit as monodisperse flow and are counted by a detector.

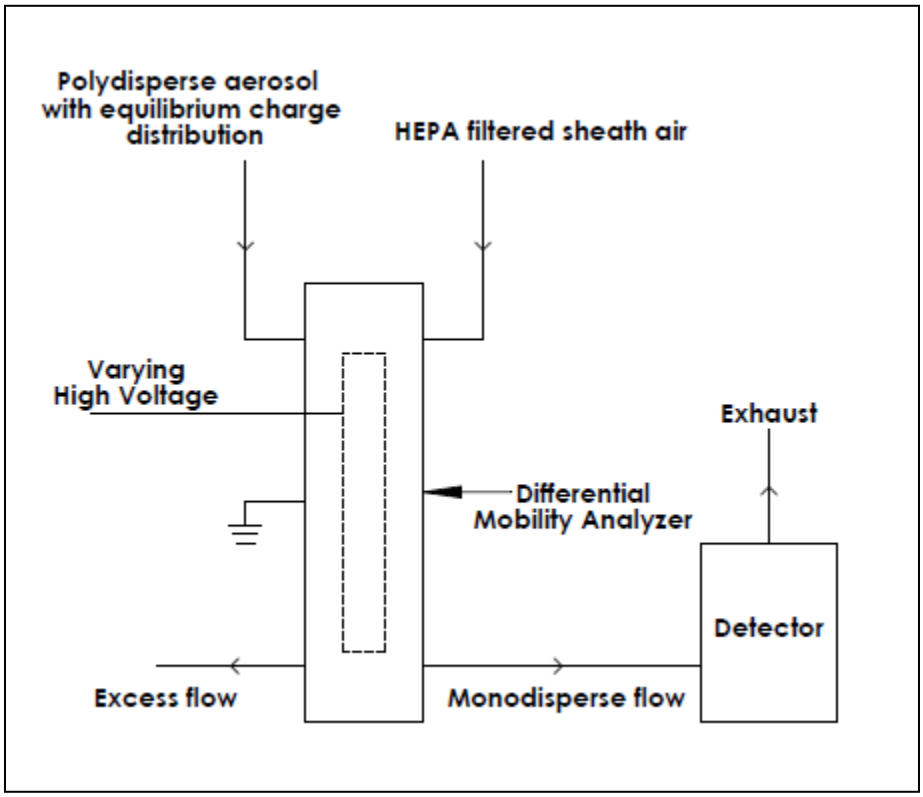

Figure 1: Schematic of Scanning Electrical Mobility Spectrometer

The theory for measuring particle size distribution using SEMS was developed by Wang and Flagan (1990). In this theory, the scanning mode of operation for determining particle size distribution is explained which is applied due to its advantages over the stepping mode of operation. This is required for aerosols whose composition changes quickly and a small size distribution measurement time is required. In the scanning mode the electric field is changed continuously and a data inversion algorithm

produces results of size distribution for the aerosol. For scanning mode of operation, continuously varying electric field at the center rod is given as

$$E_1 = E_1(t) \qquad [1]$$

It is assumed that the time during which the electric field changes is much longer than the aerodynamic relaxation time of particles and hence inertial effects can be neglected. Particles reach the extraction slot of the DMA from the aerosol inlet after a fluid residence time t_f. It is assumed that the particles would reside in the analyzer column for the same time as the fluid. After a delay of t_d from the time particles are extracted from the DMA, particles reach the detector. After time t_f+t_d, from the start of scanning process the first particle would reach the detector and all following particles would have different mobility. The instrument response functions for determining the size distribution of aerosols are derived in the following paragraphs.

Radial migration of charged particles in the DMA with a continuously varying electric field can be described by

$$\frac{dr}{dt} = Z_p E_1(t) \frac{r_1}{r} \qquad [2]$$

where Z_p is the electrical mobility of particle, and r is the radial position of the particle with respect to the center rod. A schematic showing trajectories of particles in the DMA is shown in Figure 2. Radial position of the particles that entered the analyzer at t_{in}, after a time t inside the analyzer column can be found by integrating Equation [2].

$$r^2(t_{in} + t) = r_{in}^2 + 2Z_p r_1 \int_{t_{in}}^{t_{in}+t} E_1(t')dt' \qquad [3]$$

where r_{in} is the radial position of the particle when it enters the analyzer column, and r_1 is the radii of the collection rod. On examination of the response of the instrument to particles reaching the extraction slot at $t_m=t_{in}+t_f$, it is found that particles in a range of mobility will be extracted. Here the assumptions are made that flow is uniform and radial gas velocity is negligible. The largest mobility contributing to particles will correspond to particles entering at r_2 and reach r_2 at the upstream edge of sample extraction slot. Assuming uniform axial velocity, residence time for highest mobility particles can be given by

$$t_f = \frac{\pi(r_2^2 - r_1^2)L}{Q_a + Q_{sh}} \qquad [4]$$

where Q_a is the aerosol flow rate, Q_{sh} is the sheath air flow rate and L is the length of analyzer column from center of the aerosol inlet to center of the sample extraction slot. Evaluating Equation [3] for this time the maximum electrical mobility contributing to extracted particles is

$$Z_{p,\max} = \frac{r_1^2 - r_2^2}{2\int_{t_{in}}^{t_{in}+t_f} E_1(t')r_1 dt'} \qquad [5]$$

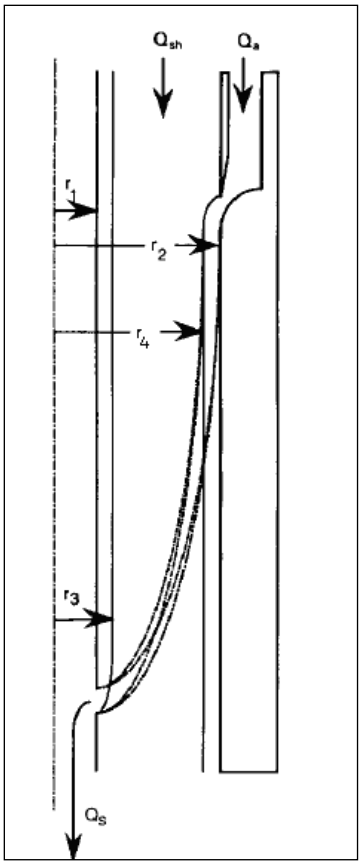

Figure 2: Particle Trajectories in Differential Mobility Analyzer (Wang and Flagan 1990)

Similarly, minimum mobility can be obtained by considering particles which enter the column at the innermost radial position r_4 and reach the end of sample extraction slot at r_3. The residence time for particles is given by

$$t_f = \frac{\pi(r_4^2 - r_3^2)L}{Q_{sh} + Q_s} \qquad [6]$$

$$Z_{p,\min} = \frac{r_3^2 - r_4^2}{2\int_{t_{in}}^{t_{in}+t_f} E_1(t')r_1 dt'} \qquad [7]$$

Only a fraction of particles entering the DMA between this mobility range will be extracted. These particles will reach the sample extraction slot at $r_1<r\leq r_3$. Particles with mobility greater than $Z_{p,min}$ will contribute to sample flow only if they are within a critical radial position r_c. Particles following this critical trajectory must reach r_3 in

$$t_f = \frac{\pi(r_c^2 - r_3^2)L}{Q_{sh} + fQ_a - Q_s} \quad [8]$$

where

$$f = \frac{(r_c^2 - r_4^2)}{(r_2^2 - r_a^2)} \quad [9]$$

where f is the fraction of aerosol flow entering the sample extraction slot with $r<r_c$. Rearranging Equation [8] and using Equation [3]

$$f = \frac{K(t_m) + Q_s - Q_{sh}}{Q_a} \quad [10]$$

where

$$K(t_m) = -2\pi r_1 Z_p L \overline{E}_1(t_m) \quad [11]$$

and

$$\overline{E}_1(t_m) = \frac{1}{t_f}\int_{t_m - t_f}^{t_m} E_1(t')dt' \quad [12]$$

A similar analysis for particles with mobility smaller than $Z_{p,max}$ gives

$$f = \frac{-K(t_m) + Q_a + Q_{sh}}{Q_a} \quad [13]$$

In case of a smaller sample flow than the aerosol flow, the fraction extracted cannot be larger than

$$f = \frac{Q_s}{Q_a} \qquad [14]$$

For any mobility Z_p, the fraction of particles extracted will be

$$\Omega = \max\left[0, \min\left(\frac{K(t_m) + Q_s - Q_{sh}}{Q_a}, \frac{-K(t_m) + Q_a + Q_{sh}}{Q_a}, \frac{Q_s}{Q_a}, 1\right)\right] \qquad [15]$$

As the field is varying continuously, critical trajectories depend upon the time particles enter the analyzer column. To eliminate this dependence an exponentially changing electric field is chosen.

$$E_1(t) = \alpha e^{\pm t/\tau} \qquad [16]$$

Substituting in Equation [3], the particle trajectory is

$$r^2(t_{in} + t) = r^2(t_{in}) + 2Z_p r_1 \alpha(\pm\tau) \times e^{\pm t_{in}/\tau}(e^{\pm t/\tau} - 1) \qquad [17]$$

And the mobility parameter for this ramping function is

$$K(t_m) = \mp 2\pi r_1 Z_p L \frac{\alpha\tau}{t_f}\left[1 - e^{\mp t_f/\tau}\right] \times e^{\mp t_m/\tau} \qquad [18]$$

It can be seen here that an exponential ramp ensures the dependence of critical trajectories and transfer function only on $K(t_m)$. In the SEMS, the electric field is varied continuously and the particles extracted are monitored using a Condensation Particle Counter (CPC). To reach the detector, the particles need to flow through the plumbing, which takes an additional delay t_d. Counts made by the CPC need to be taken for a finite time in order to obtain statistically relevant results. This counting time is t_c.

The relevant transfer function is obtained by averaging over the counting time.

$$\overline{\Omega} = \frac{1}{t_c}\int_{t_m}^{t_m+t_c} \Omega(Z_p, t)dt \qquad [19]$$

Fraction of particles of mobility Z_p extracted through the analyzer column is described by the transfer function. The mobility of particles is

$$Z_p = \frac{neC_c}{3\pi\mu D_p} \qquad [20]$$

where n is the number of elementary charges, e is the elementary charge, μ is the gas viscosity, C_c is the Cunningham slip correction factor and D_p is the particle diameter. Particles acquire an equilibrium charge distribution when they pass through a bipolar charger. The probability for a particle of diameter D_p acquiring a charge i can be predicted by Wiedensohler (1988) which is an approximation of Fuchs (1963) model and is given by

$$\phi(D_p, i) = 10^{\left[\sum_{k=0}^{5} a_k(i)\left(\log\frac{D_p}{nm}\right)^k\right]} \qquad [21]$$

where $a_i(N)$ are the coefficients for the equation and N is the number of elementary charges on particles. The detector response to particles of diameter D_p and charge i is given by $s(D_p,i)$. The instrument response is the weighted integral over counting time t_c, thus at time $t=t_m+t_d+t_c$, the response obtained is

$$S(t) = \int_0^{\infty} n(D_p)\Gamma(D_p, t_m, t_c)dD_p \qquad [22]$$

where the system response function is

$$\Gamma(D_p, t_m, t_c) = \sum_{i=-\infty}^{\infty} s(D_p, i)\phi(D_p, i)\overline{\Omega}(Z_p(D_p, i), t_m, t_c) \qquad [23]$$

A response is obtained after every interval t_c at time t_j which can be described as

$$t_j = t_d + jt_c \quad [24]$$

where j=1,2,……N.

From these measurement S_j , $n(D_p)$ is to be found.

2.1.2 General Design (Hardware Description)

The SEMS system can be separated into two sub-systems. These are the electrical system and the fluid flow system. For each system the design, operation and components are described in the following sections.

Electrical System

A schematic showing the design of the electrical system is shown in Figure 3. The arrows represent the direction of signal or current. It can be seen that the Condensation Particle Counter (CPC) is connected to the computer and High Voltage Supply (HVS). A RS 232 cable provides capability to send and receive signals between the CPC and computer. To interface the CPC with HVS, an adapter is used which connects two coaxial cables from the CPC to a DB 9 cable on the HVS. Through this interface, voltage is applied by the CPC (0.01V-10V) which acts as a programming signal and the HVS (0.01V-10V) which acts as the monitoring signal for high voltage output. For supplying power to HVS, a 24V DC power supply is connected to this adapter. Figure 4 shows a picture of the HVS to CPC adapter. A toggle switch is provided on the adapter to turn power on and off as no such function was available on

the HVS. Another adapter acts as interface between the HVS and DMA. It connects a coaxial cable with an Ultra High Frequency (UHF) connector from the HVS to the high voltage cable on DMA. A picture of the HVS to DMA adapter can be seen in Figure 5.

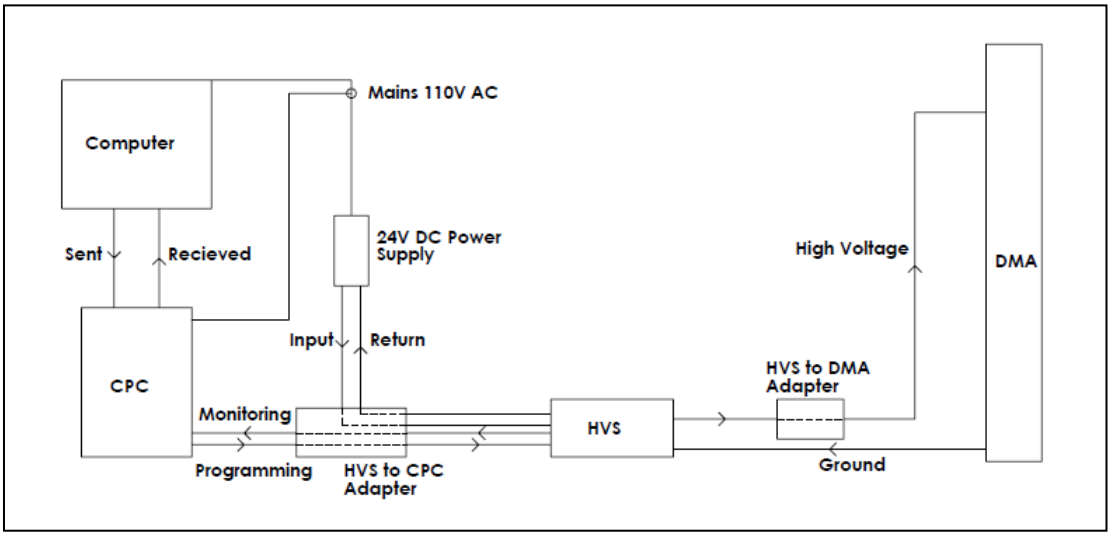

Figure 3: SEMS electrical system

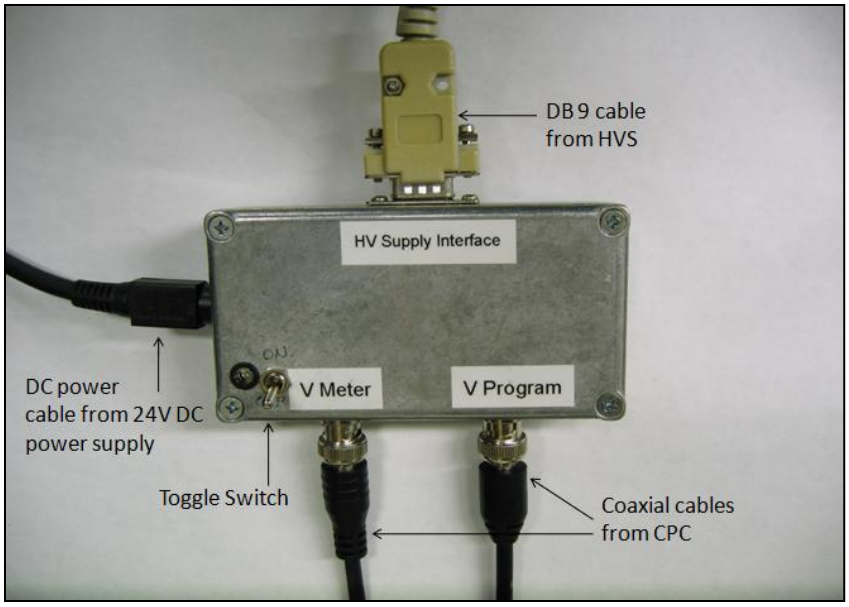

Figure 4: Interface between HVS and CPC

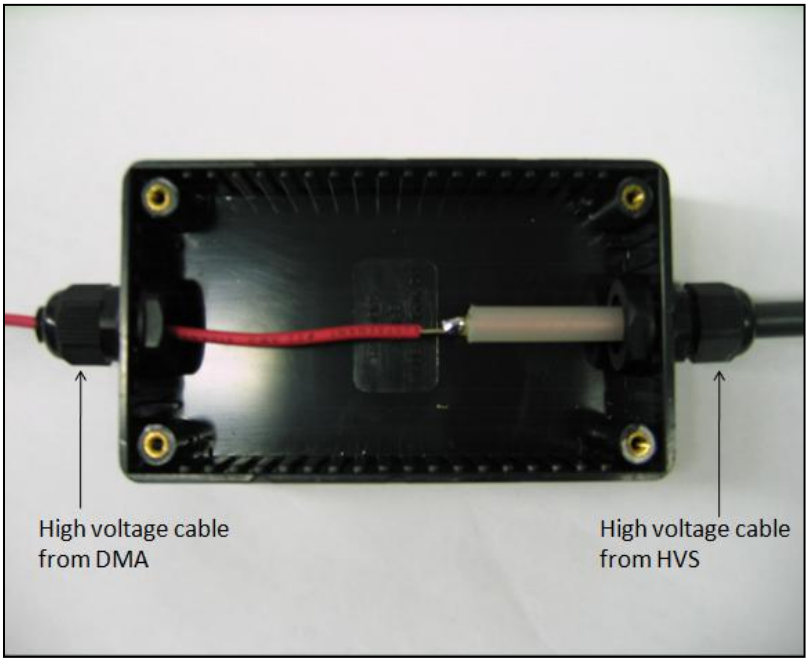

Figure 5: Interface between HVS and DMA

To describe the operation of SEMS electrical system, arrows are used which give the direction of flow of current. The computer sends a signal with the input parameters for the scan to the CPC. Once the hardware status is checked and confirmed to be ‘ok’ by the CPC, it starts a scan and in turn sends voltage signals (0.01V-10V) to the HVS. A high voltage (10V-10000V) is then generated and applied at the center rod of the DMA. This helps generate an electric field which separates particles according to their electrical mobility. During this process, signals are continuously sent to the computer from the CPC with particle count data. The DMA outer electrode is grounded through the HVS and 24V DC power supply to the mains outlet.

Fluid Flow System

The theory of SEMS operation was mentioned in section 2.1. The design to realize various functions of the SEMS can be seen in Figure 6. Main components of the SEMS system are the Differential Mobility Analyzer (DMA) and the Condensation Particle Counter (CPC).

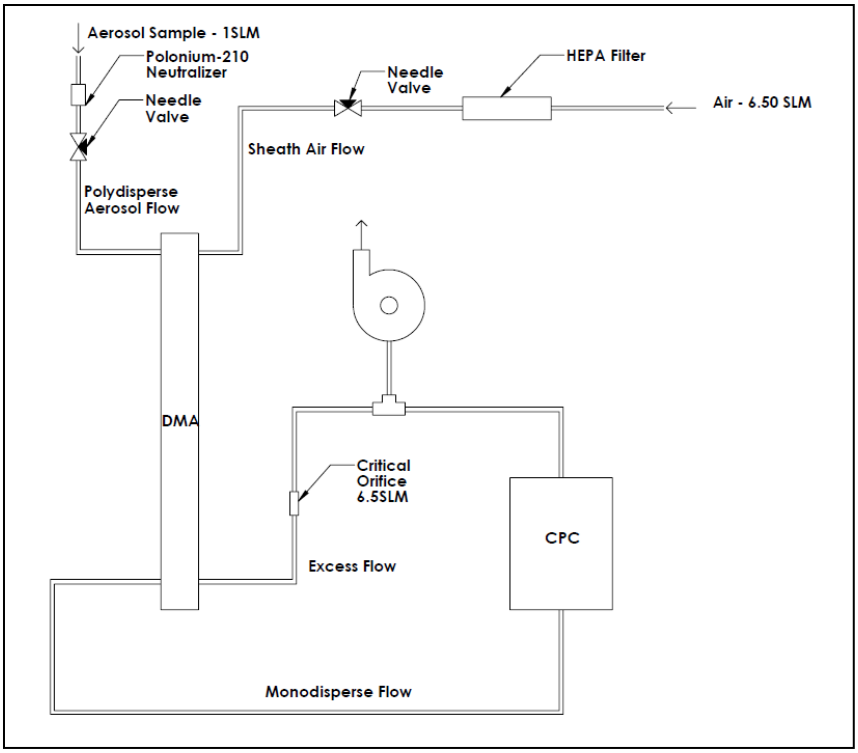

Figure 6: Schematic of the Fluid Flow System for the SEMS system

Differential Mobility Analyzer (DMA): The DMA was purchased from TSI Inc. (Model #3081) and has the capability to separate particles in the range of 10-1000nm according to their electrical mobility. It is based on the design of Knutson and Whitby (1975). The DMA consists of two cylindrical electrodes made of polished stainless steel. They are insulated from each other at the top by a Teflon spacer and at the bottom by acetyl-plastic spacer. High voltage is applied to the inner electrode which is 0.369in (0.937cm) in radius. The outer electrode is 0.772in (1.961cm) radius and distance between center of aerosol inlet and exit which is the characteristic length is 17.468in (44.369cm).

Condensation Particle Counter (CPC): Condensation Particle Counters (CPC's) are devices that grow aerosol particles to optically detectable limits and then count number of particles per unit volume of gas. They have been in existence since late 19th century and the first use of CPC was made by John Aitken (1890) to count dust particles in air. CPC's have seen a lot of development since then, and the most recent developments have focused on steady state flow CPC's. In the design of SEMS, model 3772 CPC from TSI Inc. counted particles in the aerosol. The 3772 had the capability to measure particles as small as 10nm where as it could count up to 10000 pp/cc.

CPC's are similar to optical particle counters, however smaller particles can be counted through the process of growing particles by condensation. The main science involved in CPC's is the condensation of vapor onto aerosol particles. The CPC consists of three sections: saturator, condenser and optical detector. The saturator section is made of a saturator wick which soaks butanol from a reservoir and saturates the aerosol flow. The flow then enters the condenser section where vapors get cooled and flow becomes supersaturated. This leads to condensation on aerosol particles and their growth to sizes detectable by the optical system. Finally, the concentration of particles is measured in the optical detector system using a laser diode and photo detector.

Other equipment:

1/4thinch. OD Copper tubing is used to transport aerosol in the Fluid Flow System. To control flow in the system, two needle valves (Swagelok) and a 6.5 SLM critical orifice from O'Keefe Controls Co. were used. Compression fittings were used at all interfaces which prevents outside air from entering the system due to system vacuum.

For the filtering of sheath air, a HEPA filter of pore size 0.22micron was applied as seen in Figure 6. Finally, Thomas Products (Model # 2688VE44) pump provided vacuum to the SEMS system.

A Polonim-210 strip from AMSTAT Industries Inc. (500 Microcurie) encased in a stainless steel cylindrical casing provided a known bipolar charge distribution to the aerosol particles. As Polonium-210 is radioactive, it releases alpha particles which ionize the air molecules in the casing. As the aerosol particles pass through the casing they acquire a known charge distribution which can be predicted by Fuchs Equation mentioned in Section 2.1.1.

Components discussed above were integrated to form the Fluid Flow System which is shown in Figure 6. Polydisperse aerosol sample enters the DMA through the polydisperse flow inlet located at top of the DMA. The flow is controlled at 1SLM by a needle valve and the bipolar charger adds a known charge distribution to the aerosol. Simultaneously, sheath air is being pulled into the DMA through the sheath air inlet after undergoing filtration. A high voltage applied at the center rod aids in attracting particles within a narrow range of mobility which exit through the monodisperse flow outlet at 1L/min. The monodisperse aerosol then flows through the CPC where the particle concentration is determined. Finally, the remaining aerosol flows out through the excess air outlet along with sheath air and meets the monodisperse aerosol exhausted from the CPC. The excess air flow is controlled by a 6.5SLM critical orifice. The flow is finally exhausted through a pump to the fume hood.

2.1.3 SEMS Software

Once the hardware setup was complete, the second major constituent of SEMS system was its software. Its main function was to connect the user and the hardware by interfacing with them. A theoretical model for the SEMS software can be seen in Figure 7.

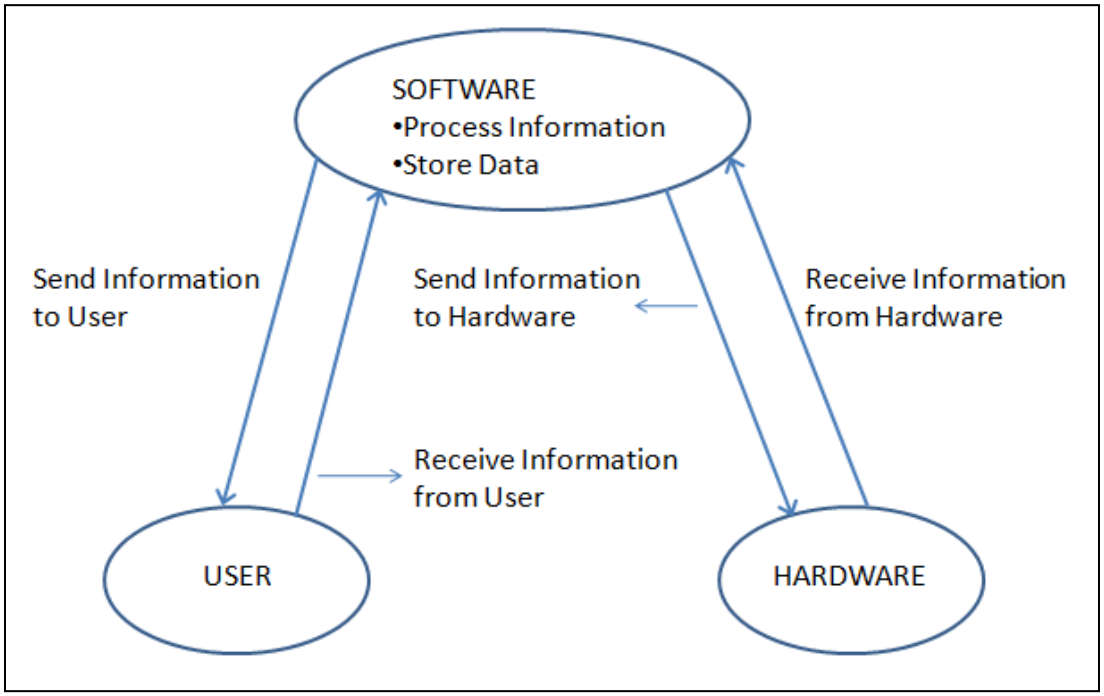

Figure 7: Software model for the SEMS system

The software received input from the user and communicated it to the hardware to start a scan. The software continuously received data from the hardware and

processed and stored it. Once the scan was complete, the software displayed particle size distribution results graphically and stored scan data.

The main theory mentioned in section 2.1.1 applies to the SEMS software and includes the inversion of raw concentration data obtained from the CPC to the actual concentration of particles in aerosol and plot a size distribution function. The size distribution function can be produced by joining the values of size distribution function at various particle diameters obtained experimentally. For particles smaller than 100nm, most charged particles carry only a single charge. Therefore, Equation [22] simplifies to

$$S_j = \int_0^{\infty} n(D_p)s(D_p,1)\phi(D_p,1)\times\overline{\Omega}(Z_p(D_p,1),t_m,t_c)dD_p \qquad [25]$$

Since particles in a narrow range of mobility are extracted at any given time, $n(D_p)$, $s(D_p,1)$ and $\phi(D_p,1)$ can be assumed to be constant. The value of the size distribution function for any time step j is

$$n(D_{p,j}) \approx \frac{S_j.\frac{dZ_p}{dD_p}}{P.s(D_{p,j},1).\Phi(D_{p,j},1).\int_{Z_p-\Delta Z_p}^{Z_p+\Delta Z_p}\overline{\Omega}(Z_p,t_m,t_c)dZ_p} \qquad [26]$$

In this equation P has been included to signify the penetration losses in the tubing from the aerosol inlet probe to the detector.

The software and hardware communicates through a RS-232 cable. The CPC has an inbuilt microcomputer with firmware commands to control various functions. An algorithm was designed in MATLAB which was able to communicate with the CPC,

process data and display results to the user. Figure 8 shows the algorithm which is discussed in the following paragraphs.

In the first step, user-defined variables are requested. These include variables such as the scan time, scan voltage range and the sampling tube length. The sampling tube length is the length of tube from extraction probe, to DMA aerosol inlet (polydisperse aerosol inlet). The mobile design of SEMS system allows aerosol testing from different environments for which different tube lengths are used. Parameters that remained constant are defined next. Among others, these include constants such as the inner and outer radii of the DMA and constants for various equations such as those used to determine the counting efficiency of CPC and charging probability for particles.

Next, blank vectors are created to hold the data generated during the scan. Each vector is a column vector with size equal to the scan time. Data is generated for each time step which is one second; therefore, the number of data elements was equal to the total time for the scan. Before initiating the size distribution scan, user-defined variables are conveyed to the CPC. These include parameters such as the scan time, voltage range, a choice between up scan and down scan. By checking the status of the hardware, it was confirmed that the operating ranges were accurate. Temperatures of optics, condenser and saturator are observed along with the Butanol level. If any variables are determined to be out of range, the user is asked whether the scan is to continue. The user can then decide to continue with the measurement, or correct the upset variables.

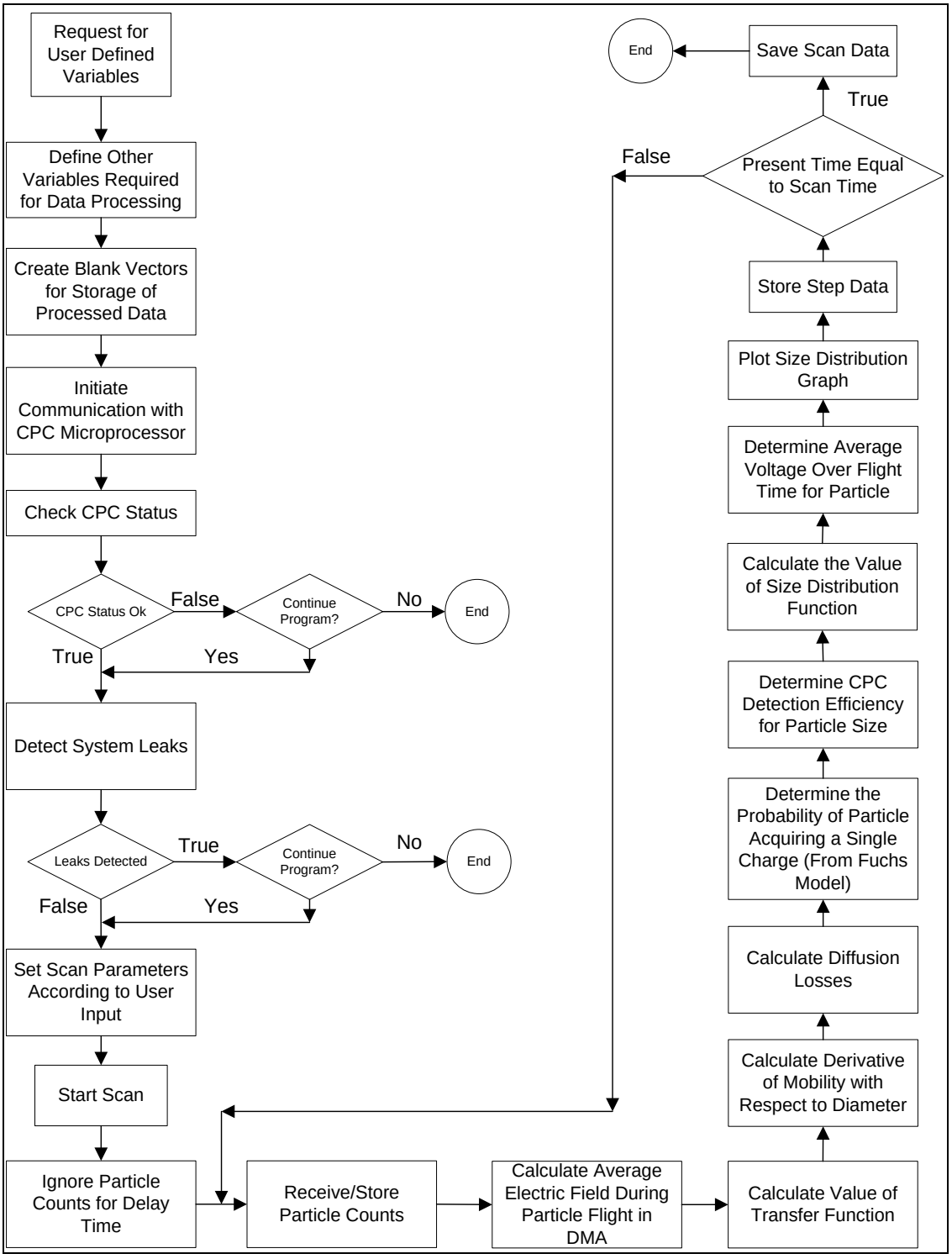

Figure 8: SEMS algorithm flowchart showing the program design to obtain particle size distribution of aerosols

The next step in the algorithm involves detecting leakage status in the hardware. Sheath air passes through a HEPA filter before entering the system. This leads to particle free air and when no voltage was applied at the DMA, the particle concentration is observed to be zero. Due to vacuum in the system, a leak in the plumbing would cause particles other than the aerosol particles to enter the system. The concentration is increased due to this and often results in overshooting the detectable range of CPC. Concentration is averaged over a period of five seconds. If the concentration is below 0.1pp/cc, the program moves to the next step. Otherwise, the user is provided the option of discontinuing the program and checking the hardware for leaks. Once the scan is initiated, a time delay exists between particles exiting the DMA monodisperse outlet and reaching the CPC particle detector. These particles travel through the interfacing plumbing and internal CPC tubing. The delay time was found to be 0.507 seconds. All particles detected by the CPC counter are thus ignored during this interval.

In the next step of the algorithm, the computer receives and stores particle count data in the blank vectors created earlier. The CPC counts particles every 0.1 seconds and sends these values to the program buffer. The program receives these values and averages counts over 1 second, to find the particle concentration. The particle concentration data is then combined with other parameters for each time step to determine the size distribution function, as discussed in the following paragraphs. Worthy of mention in this process was gaining an understanding of the process of receiving the particle counts from the CPC microprocessor. A first attempt at receiving information from the CPC was made by considering that firmware commands are

required to acquire particle counts. Erratic data received after implementing a number of firmware commands resulted in temporary discontinuation of real-time size distribution analysis. A Microsoft Excel spreadsheet was developed with data inversion algorithm. Particle counts obtained through separate software are integrated within the algorithm for obtaining offline size distribution measurements. Due to lack of automation, this process proved to be time consuming and it was decided to gain deeper understanding of the process of receiving counts from the CPC microprocessor. After a number of trials, the process of receiving particle counts was realized. Particle counts are sent by the CPC microprocessor to the software buffer, which is a temporary storage for external data. The temporary data is collected by the SEMS software as it becomes available and stored in a blank vector as discussed earlier. Once particle counts are received by the software, the rest of the parameters required for data inversion are processed internally. The average electric field is found using Equation [12]

$$E_1(t) = \frac{V(t)}{r_1 \ln(r_1/r_2)} \qquad [27]$$

Finding the average electric field involves determining the voltage ramp function executed by the CPC. This is done by recording the ramping voltage at the CPC analog outlet using a multimeter and curve fitting the data to obtain an equation for the voltage ramping function. Equation [28] shows this relation.

$$V(t) = SV \exp\left(\frac{t}{\tau}\right) \qquad [28]$$

Here, V(t) is the voltage at time t, SV is the start voltage and τ is the time constant and is defined in Equation [29].

$$\tau = \frac{ST}{\ln\left(EV/IV\right)} \qquad [29]$$

where ST is the scan time, and EV is the end voltage. Only a fraction of particles entering the DMA through the aerosol inlet, exit the DMA as monodisperse flow. For every time step, this fraction was expressed by determining the transfer function as for a range of mobility as shown in Equation [26]. Again the values of the transfer function and average electric field were stored in the column vectors.

Diffusion losses take place in the plumbing while particles travel from the DMA outlet to the particle detector. Particles lost to the walls of the tubes through diffusion can be accounted for by finding the fraction of particles that exit the tubes (Hinds 1999). This is given by:

$$P = 1 - 5.50\xi^{2/3} + 3.77\xi \qquad \text{for } \xi < 0.009$$

$$P = 0.819\exp\left(-11.5\xi\right) + 0.0975\exp\left(-70.1\xi\right) \qquad \text{for } \xi \geq 0.009 \qquad [30]$$

where ξ is the dimensionless deposition parameter and can be defined as:

$$\xi = \frac{DL}{Q} \qquad [31]$$

where D is the diffusion coefficient, L is the length of tubing and Q is the aerosol flow rate in tubing.

Finally, particles are charged in a Bipolar charger leading to a particle of diameter D_p acquiring a charge i of $s(D_p,i)$. Assuming single charge on the particles, Fuchs' model can be used to predict the charging probability. Equation predicting the

charge probability is given by [21]. Assuming single charging probability, the coefficients are given in the Table 1.

Table 1: Coefficients for Fuchs' Equation

a_i (N)	a_0	a_1	a_2	a_3	a_4	a_5
N=1	-2.3484	0.6044	0.4800	0.0013	-0.1553	0.0320

The CPC has different counting efficiencies depending on particle sizes. The counting efficiency curve obtained as an average of three trials, was provided by TSI, Inc. and can be seen in Figure 9.

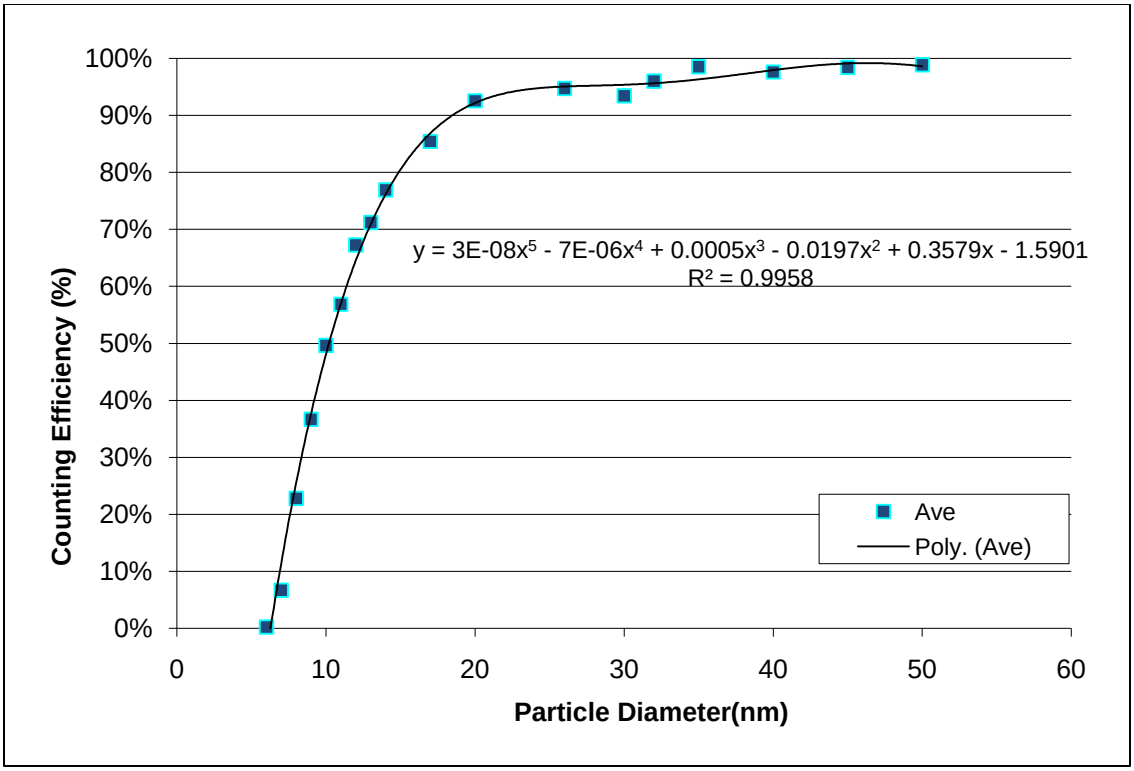

Figure 9: CPC 3772 detection efficiency with respect to particle diameter (Shown here with permission from TSI Inc.)

Finally, Equation 26 is used to calculate the value of the size distribution function for the time step. This process is continued until the time equal to the scanning time has passed. To display the results to the user, a graph containing raw count data versus applied voltage and size distribution curve was generated, an example of which is shown in Figure 10.

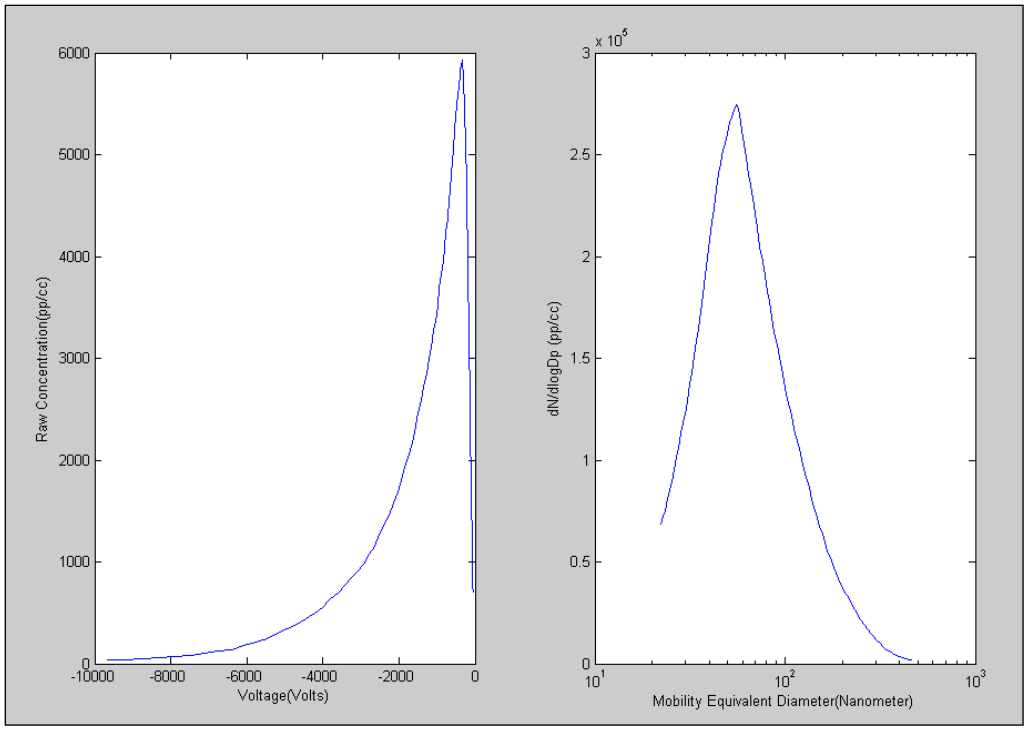

Figure 10: Example of graphical representation of particle size distribution by SEMS. Graph shows size distribution of particles in atomized aqueous suspension of 6mM TiO2 + 0.106mM Tween-20

2.2 Calibration

2.2.1 Experimental

To establish a precise relation between high voltage output and the programming voltage the unit was calibrated. The programming voltage which is provided by the CPC to the HVS was tested first to see if the voltage set by computer on the CPC was equal to the programming voltage output to the HVS. This was done by setting a voltage on the CPC using the computer and measuring the actual programming voltage output by the CPC

analog output port. Once it was confirmed that the CPC set and output voltage values were equal, the relation between CPC output voltage (0.01V-10V) and the HVS output (10-10000V) was determined. Although information provided by the HVS manufacturer indicates that the relation is HV=1000PV where PV and HV are the programming voltage input and high voltage output respectively, this was not the case. A multimeter measured high voltage output from HVS while the CPC provided the programming voltage to it. The programming voltage on the CPC was set through the computer using firmware commands for the CPC microcomputer. As the highest voltage measured by the multimeter was 600V, the relation between PV and TV up to 600V of high voltage output was assumed to hold true for the entire range.

Testing the high voltage supply was required to confirm the actual range of voltages that it was functional in, as opposed to the given specifications. Along with this, an appropriate scan time needed to be determined in which a significant lag would not be observed between theoretical ramping function and the actual high voltage. The minimum functioning voltage was found by experimentally determining the settling time for an increment of 10V from the minimum voltage. This was the time between setting a voltage at the CPC and getting a stable output from the HVS. The criterion for selection of minimum voltage was that the settling time would be less than 5 sec. The minimum functioning voltage was 42V and it took approximately 3s to reach a stable value of 52V at the HVS output.

The Fluid Flow System was pressure tested to prevent any leaks in the system. A leak could lead to particles from ambient air entering the system and skewing the size distribution. To check the classifier for leakage, a pressure test was conducted in which all the plumbing lines including the DMA were pressurized. A pressure/vacuum gauge was attached to the lines as in Figure 11 to check if the pressure decreased with time. 25 psi of pressure was applied using a pressure pump. Before starting the pressure pump, the needle valve was opened very slightly to avoid rapid increase in pressure inside the DMA. Once the pump had started, the needle valve was opened slowly and the pressure was allowed to increase to 25psi. The needle valve was then closed completely so as to make system pressure tight. The pump was switched off at this point, and the system was allowed to stand for five minutes. After a few attempts and reinstallation of compression fittings it was possible to seal the classifier completely such no pressure drop was observed.

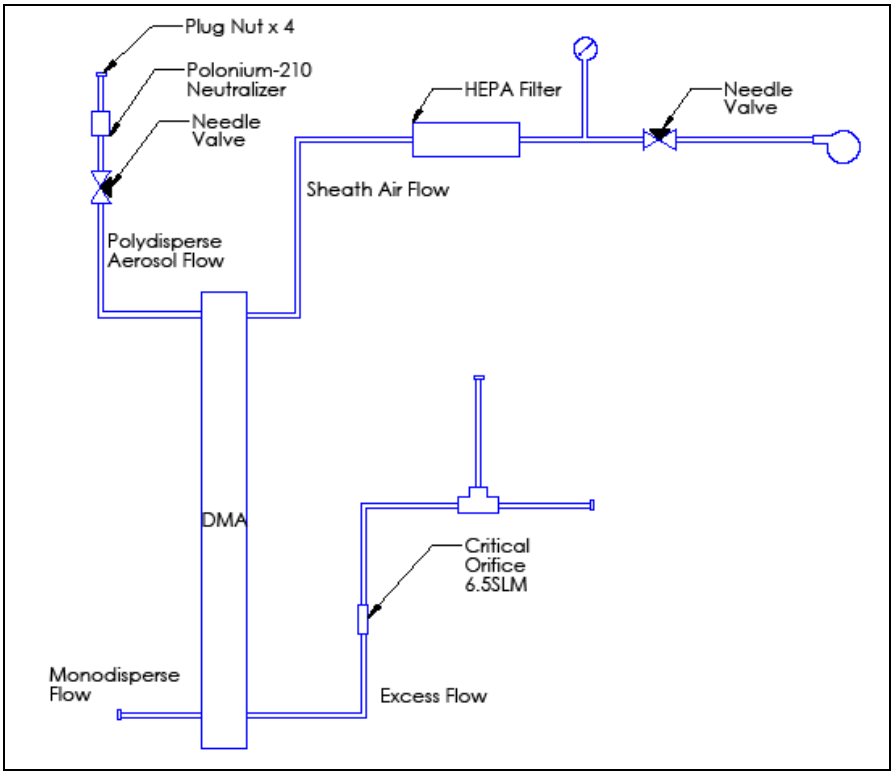

Figure 11: Setup for pressure testing the classifier for leakage

The SEMS was calibrated by measuring two sizes of Polystyrene Latex (PSL) particles. PSL particles of 99nm and 204nm (Ladd Research) were present in concentrated suspension with 0.2% (w/w) solids. The 99nm PSL suspension was prepared by keeping the concentration of PSL at 0.009mg/ml which corresponds to one particle per droplet generated by a nebulizer. For preparation of the 204nm PSL suspension, the concentration of PSL was 0.082 mg/ml which corresponded to a little less than half the mass required for one drop one particle model. This was because the quantity of PSL concentrated suspension required for one particle per drop was large. Additionally, unevaporated water droplets which might be measured by SEMS are

within the range of 10-80nm and would not interfere with size distribution of 204nm PSL particles.

The apparatus was divided into two parts; PSL particles were aerosolized in the aerosol generation system while the SEMS system measured the size distribution of PSL particles. Figure 12 shows a schematic of the setup for calibration. Compressed air passes through a HEPA filter while a multi-stage pressure regulator decreases the delivery side pressure to 20 psig. The air entered a Collison nebulizer (BGI Instruments Model# CN 241) and exited along with atomized suspension droplets at a flow rate of 2 LPM. A layer of water existing on the surface of PSL particles was evaporated by giving sufficient time before the particles entered the sampling tube and diluting the aerosolized mixture with 4LPM of filtered air. An evaporation cylinder as seen in Figure 13 was filled with desiccant to absorb excess water vapor in the air and help in evaporation of the water on particle surface. Particles were then analyzed by the SEMS to find their size distribution. Sheath air flow rate was maintained at 6.5 SLM while the aerosol flow rate was 1 SLM.

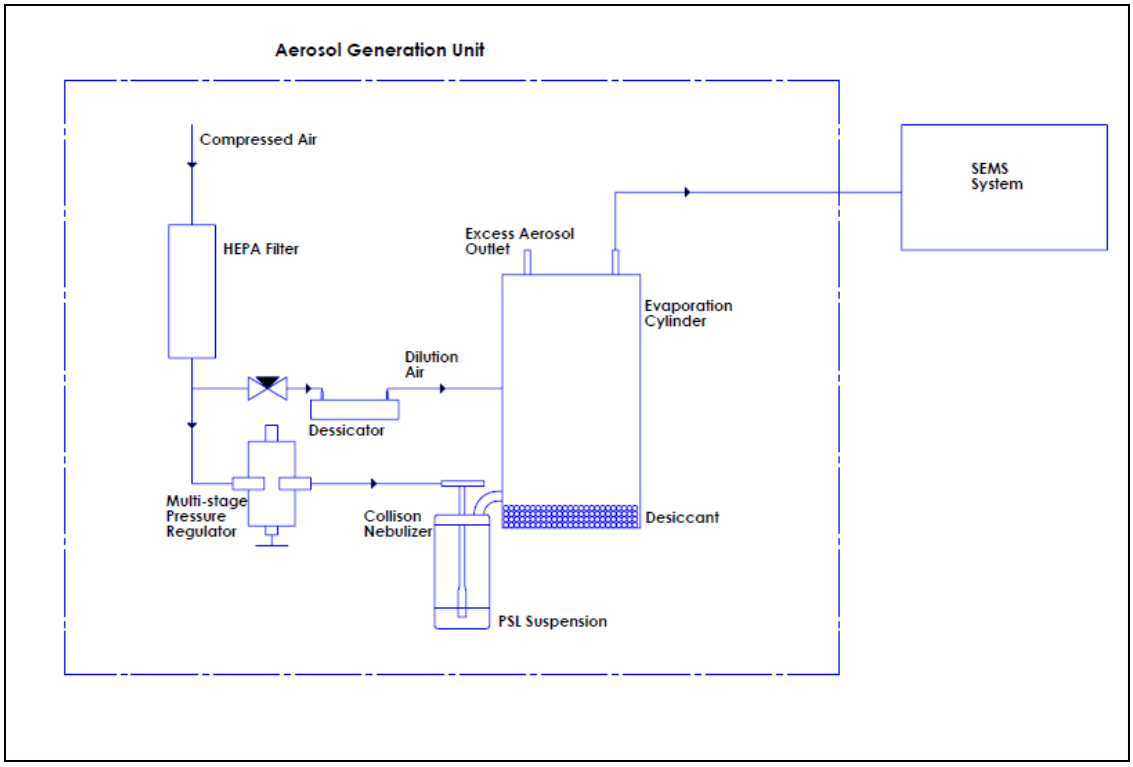

Figure 12: Apparatus setup for SEMS Calibration

The size distribution measurements of PSL suspension were taken four times for each suspension. The average mode was then computed from these trials which represented the diameter of particles at which largest particle number concentration existed. To determine the mode diameter in actual concentrated suspension, TEM analysis was conducted. For this, concentrated suspension was kept on a TEM grid and dried. TEM images were taken for both PSL particle sizes. Particle diameters were manually measured for individual particles, and the size distribution was found. The mode diameter from TEM analysis was then compared to the mode diameter obtained from SEMS measurement.

2.2.2 Results and Conclusions

Equation [32] shows the relation between HV and PV.

$$HV = 992.67PV - 27.49 \quad [32]$$

As high voltage supplies respond slowly near the higher and lower limits of voltage, a maximum voltage of 9000V was assumed as the upper limit of the HVS. By reading the responses of HVS with various scan times, 95sec was the minimum time which prevented significant lag between theoretical and high voltages. A graph comparing the theoretical and high voltage responses is shown in Figure 13. Here the theoretical response is the CPC ramping function which was applied in the program to invert data. The average difference between theoretical and high voltage was approximately 6% with higher difference close to the starting voltage in the scan. It can be concluded from this calibration experiment that the high voltage output from HVS follows the theoretical voltage closely.

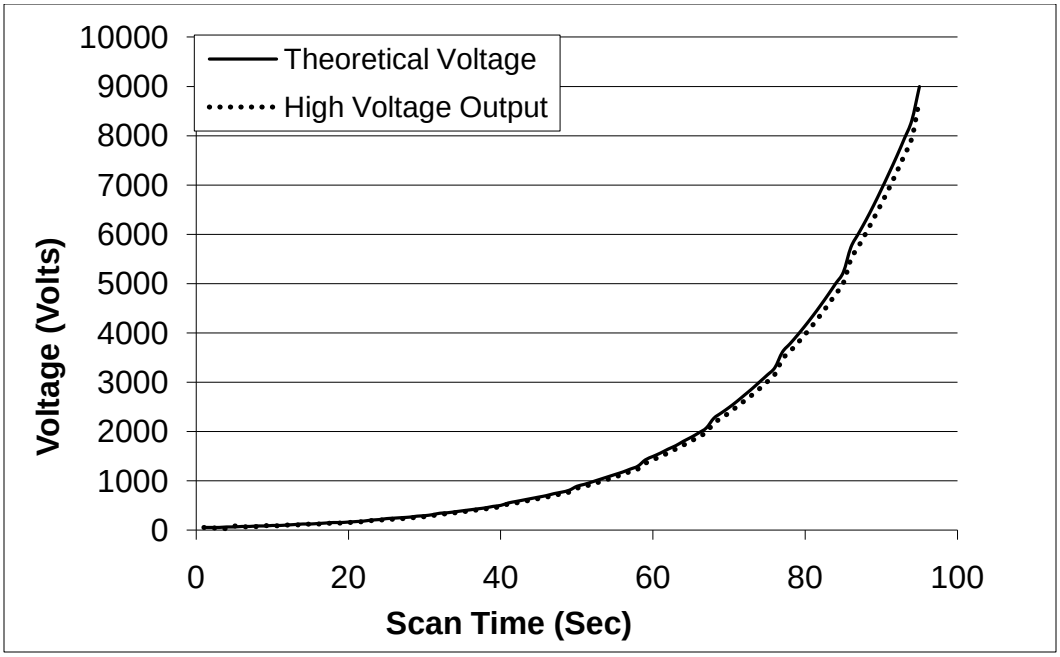

Figure 13: Comparison of theoretical or programming voltage provided to HVS and its high voltage response

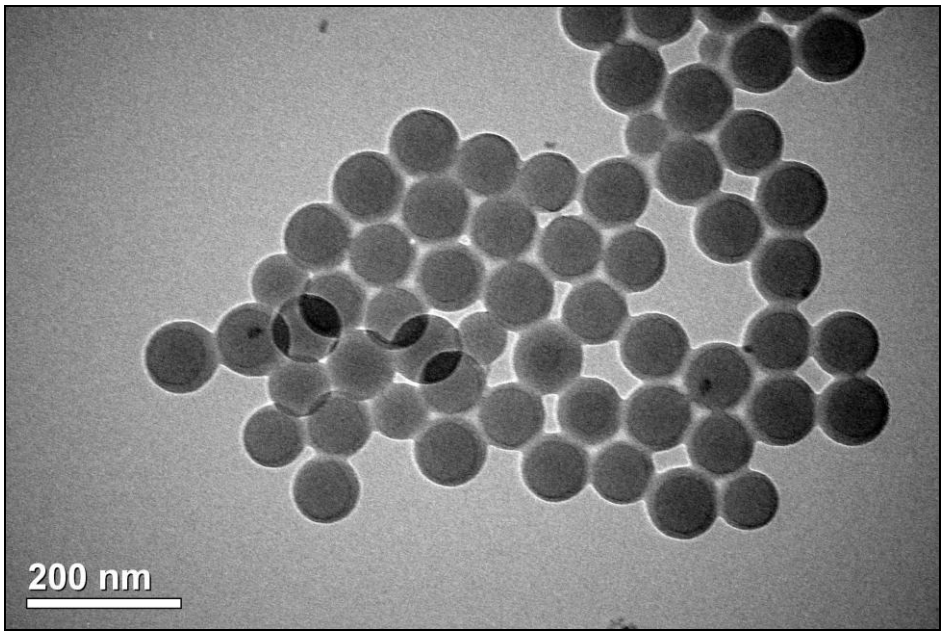

Figure 14: TEM image of 99nm PSL particles

Figure 14 shows the TEM image of 99nm nominal diameter PSL particles. A size distribution analysis of the particles revealed that the mode of particles existed at 92.5nm. A similar analysis done for 204nm nominal diameter PSL particles determined the mode diameter to be 194.9nm. Figure 15 shows an image of 204nm particles.

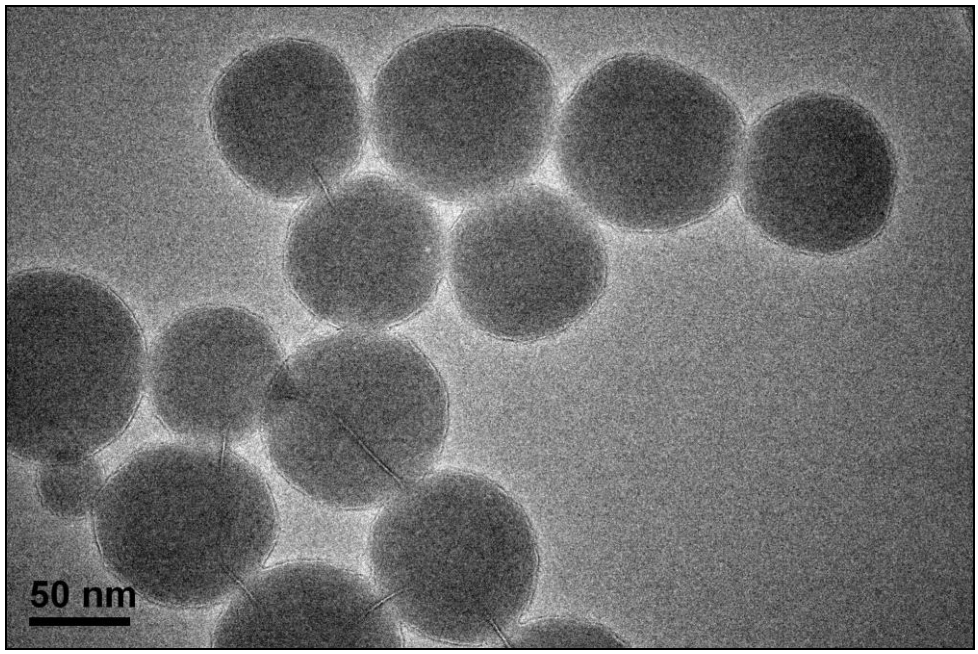

Figure 15: TEM image of 204nm PSL particles

The measurement of aerosolized PSL particles can be seen in Figures 16 and 17. The average mode diameter from four trials for nominal 99nm PSL particles was 95.8nm with no deviation from the average mode in any of the trials. Similarly, average mode diameter of 204nm PSL particles was determined to be 191.0nm by the SEMS. The error in determination of mode by SEMS system was 3.6% for 99nm particles and 2.0% in 204nm particles. Uncertainty in the control of experimental parameters such as sheath air

flow rate, aerosol flow rate and voltage which might be responsible for the error in SEMS results and TEM.

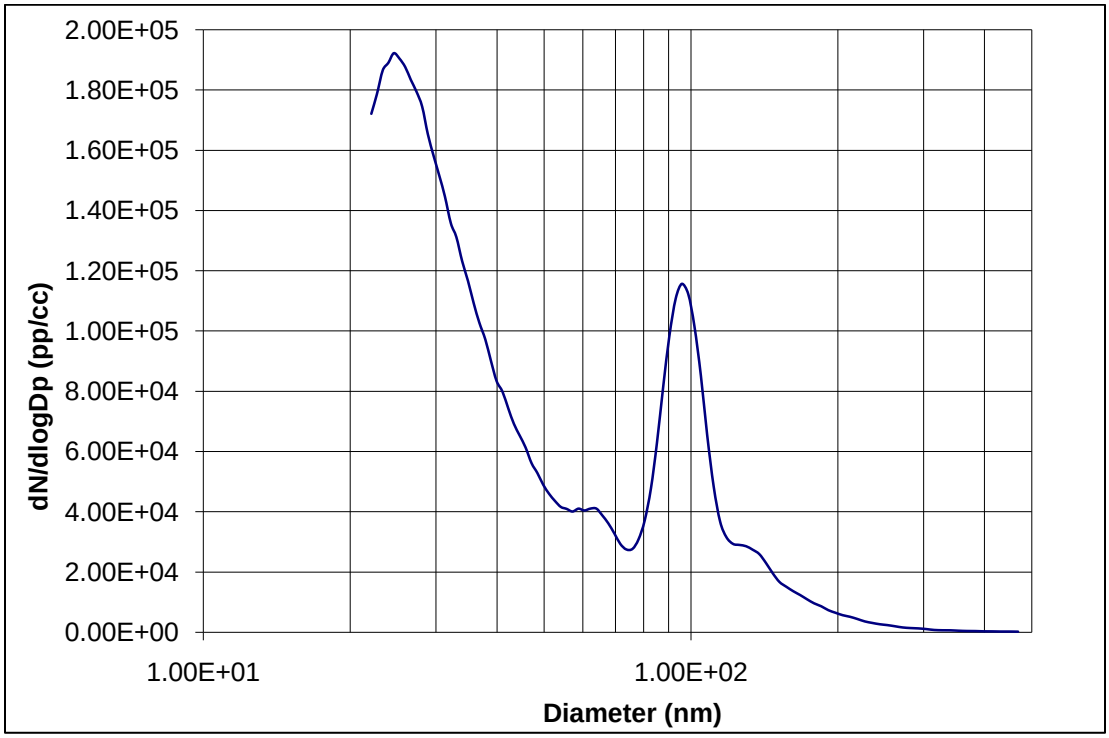

Figure 16: Particle size distribution of 99nm PSL particles as measured by SEMS system

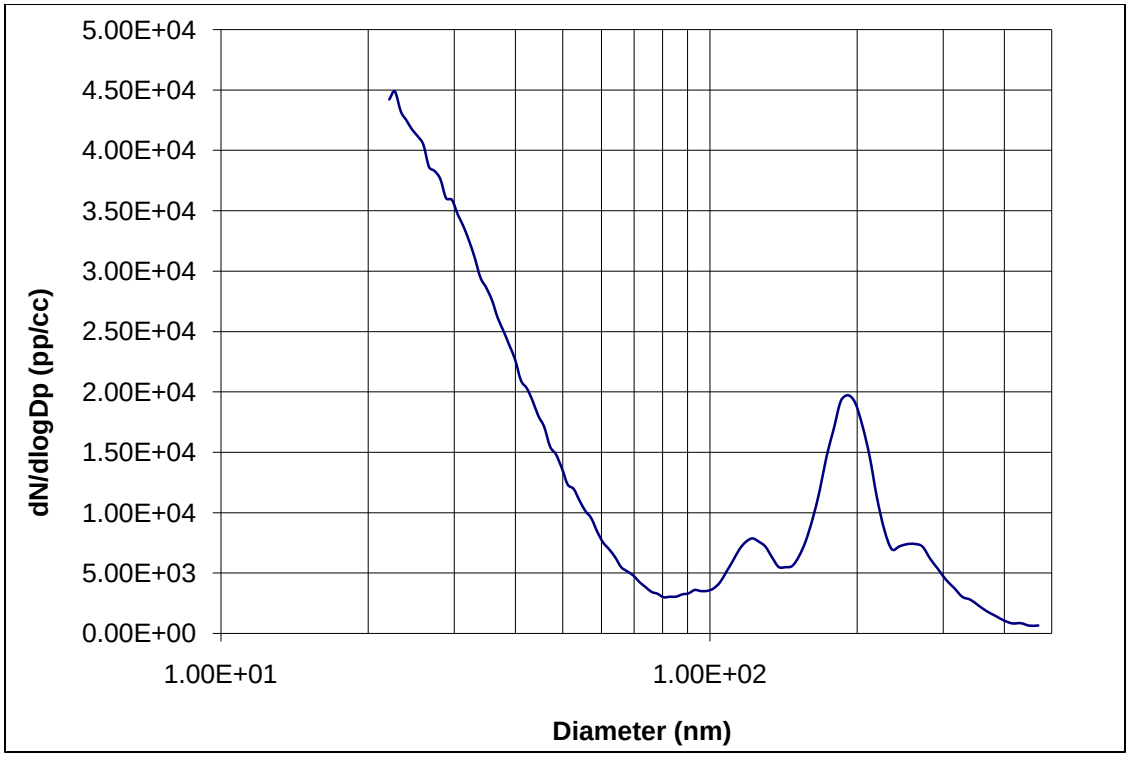

Figure 17: Particle size distribution of 204nm PSL particles as measured by SEMS system

Along with the 99nm and 204nm peaks in the measurement, peaks were also observed at 63.1nm and 130nm for 99nm PSL particles and, 122nm and 262nm for 204nm PSL particles. The peaks at higher diameters for both cases belong to singly charged doublets, while the peak at lower diameters was attributed to doubly charged single particles. A comparison between experimental results and theoretical calculations of these mobility equivalent diameters is shown in Table 2. The error in calculated and experimental values can be explained by uncertainty in experimental parameters such as sheath air flow rate, aerosol flow rate and the voltage.

Table 2: An explanation for additional peaks observed in size distribution of 99nm and 204nm PSL particles

Particle Description	Experimental Mobility Equivalent Diameter (nm)	Calculated Mobility Equivalent Diameter (nm)	Percentage Difference (%)
99nm			
Singly charged Doublet	63.1	67.2	6.1
Doubly charge single particle	130	132	1.5
204nm			
Singly charged doublet	262	269	2.6
Doubly charge single particle	122	132	7.6

It is observed in Figures 16 and 17 that certain particles are observed before the PSL particles. These particles are due to aerosolized de-ionized water and surfactants present in the PSL suspension (Zhang et al. 1995). Particles in De-ionized water will be discussed in greater detail in a later section.

3. A STUDY OF GENERATION OF TITANIUM DIOXIDE PARTICLES USING A COLLISON NEBULIZER

3.1 Introduction

Development and research in nanotechnology has accelerated since its first application of IBM logo depiction (Hood 2004). Nanoparticles exhibit a number of unique physical and chemical properties due to their large specific surface areas (Shimada et al. 2009). Due to their properties nanoparticles have found application in a number of different fields such as medicine, agriculture, industry, environment and engineering (Navrotsky 2000). For example, magnetite is used to make ferrofluids, which can be used as nanoelectromechanical (NEMS) systems, such as nanomotors, nanopumps, nanogenerators and nanoactuators (Zahn 2001). Selective manipulation and probing of biological systems can be accomplished by nanoengineered magnetic particles (Reich et al. 2003).

As with all new technologies, along with potential benefits there are a number of risks involved in nanotechnology. The risks can be to the environment and humans. For example, there is risk of exposure to the entire ecosystem through water and soil. Furthermore, the concentration of engineered nanoparticles increases in direct proportion to their use in society. Toxicology studies of micron-sized particles have been done extensively in medical studies. The coal miner's disease and asbestosis are two examples of diseases caused due to inhalation exposure to micron-sized particles. It has been

found that the nanoparticles are more toxic than micron-sized particles in similar doses due to their smaller size (Colvin 2003).

Due to risks of nanotechnology and exposure to nanoparticles, there has been increased concern about the health effect of nanoparticles. Manufactured nanoparticles exist mostly in suspension or dry powder form (Shimada et al. 2009). For inhalation exposure studies of nanoparticles, a constant supply of nanoparticles with size distribution similar to original powder or suspension is required.

In this study, the Collison nebulizer was studied as a source of nanoparticle generation from suspensions. The size distribution and concentration stability of Titanium dioxide particles generated by the nebulizer were studied and compared against single particle size distribution present in powder form. Surfactants are known to modify the interaction potential of particles in a suspension and hence give stability and increasing repulsive force between particles(Schick 1967). In this study, the effect of surfactant on particle size distribution of TiO_2 was also analyzed.

3.2 Theory/Model

The model to study aerosol generated by a Collison nebulizer is shown in Figure 18. Liquid droplets containing powder particles can be generated by a nebulizer and allowed to dry in a drying tank. The size distribution of dry particles could then be measured using a SEMS system. The Collison nebulizer breaks a stream of liquid into minute droplets. These droplets are impacted against a glass jar and only the smaller ones escape

to the exit nozzle. The concentration of powder in the suspension can be such that each droplet contains only one particle. This was done so that the aerosol generated had similar size distribution as the single particles in powder.

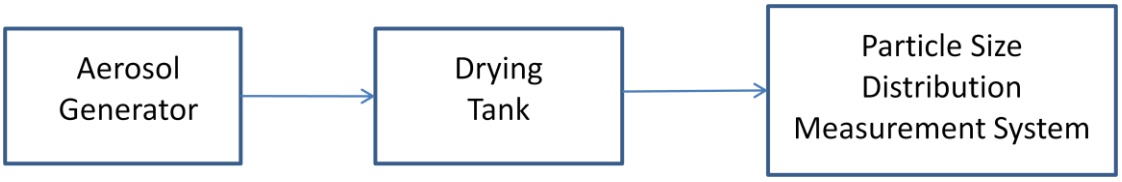

Figure 18: Model for study of aerosol generated by Collison nebulizer

From a known size distribution of droplets generated by the Collison nebulizer, it is possible to calculate the average size of droplet generated by the nebulizer. A drying cylinder which provides sufficient residence time to dry the particles can be used to produce completely dried particles whose size distribution is measurable by the SEMS system. To study the aerosol generated by the nebulizer this model was applied and is explained in detail in the following sections.

3.3 Experimental

The experimental setup for measurement of the size distribution of Titanium dioxide particles is shown in Figure 19. A Collison nebulizer (BGI Incorporated Model# CN 241) nebulized TiO_2 particles from suspension in the glass jar. Compressed air was provided to the nebulizer at 20psi after filtering it through a high efficiency particulate air (HEPA) filter. The pressure was regulated by a multi-stage regulator which delivered

filtered air at 20psi. At 20psi, the output aersol flow rate was 2LPM. Next, the aerosol entered the evaporation cylinder where dried particles were produced. The cylinder consists of two outlets for excess aerosol (1LPM) and the aerosol used for sampling by the SMPS (1LPM). A dessicant (Anhydrous Calcium Sulphate) at the bottom of the cylinder absorbed excess water vapor in the cylinder to allow evaporation of water from particles. The particles were then measured by the SEMS system.

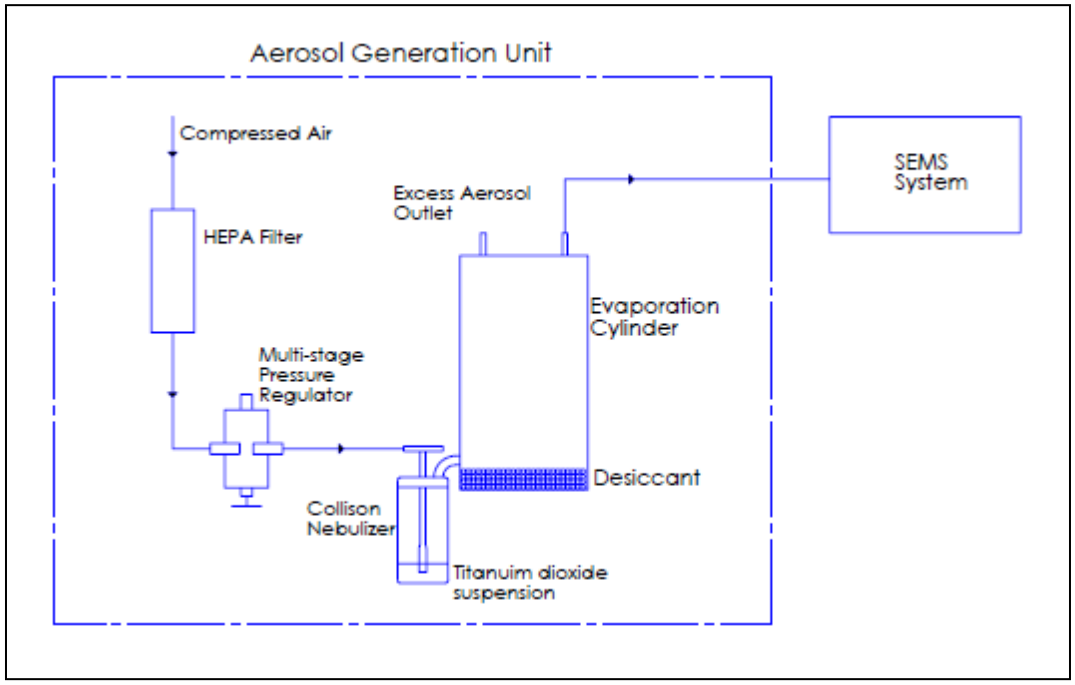

Figure 19: Apparatus setup for measuring particle size distribution of Titanium dioxide particles generated by a Collison nebulizer

The Collison nebulizer has a known size distribution output which according to empirical results obtained by BGI Incorporated has a count median diameter (CMD) and geometric standard deviation of 0.889 μm and 1.8 respectively. From these values, the

average size droplet was found to have a diameter of 4.49 μm. For this droplet, it would take approximately 3 seconds to dry completely at a relative humidity (RH) of 96.7% which was found experimentally using a humidity meter. The value of RH was noted after a stable condition was reached and the RH did not change more than 0.2% for more than 5 minutes. A residence time of 93.9 seconds inside the drying cylinder ensured sufficient time for even the larger particles to dry completely before being sampled by the SEMS.

The solution was made such that each droplet contained one particle of TiO_2 the calculation for which can be seen in the Appendix. It was found that 0.08mg/ml or 1.06mM of TiO_2 was required for each drop to contain one particle. A range of concentrations of TiO_2 were chosen to study the aerosolization of TiO_2 suspension. These ranged from 0.5mM to 9mM. Size distribution measurements of 5 concentrations of TiO_2 suspensions were made which included 0.5mM, 1mM, 3mM, 6mM and 9mM. Five size distribution measurements for each concentration were taken to observe trends in the size distribution with time. To compare size distribution of aerosolized particles with single particles present in powder, TEM was conducted as well. Particles below 30nm were not included in the size distribution analysis due to their large quantity and undefined boundaries. Most of the particles were either under larger particles or in clusters such that their boundaries were not clearly discernible in the TEM image.

To observe the aggregation of TiO_2 particles in the solution, Dynamic Light Scattering (DLS) measurements were conducted with a 1mM suspension. DLS measurements are useful in determining the size distribution of particles in a suspension.

The suspension to be sampled for DLS was probe sonicated for 5 minutes and separated into two parts. While the size distribution of the first sample was taken immediately, the other sample was nebulized using a Collison nebulizer for 30 minutes. The results of these studies can be seen in the next section.

To check the effect of surfactant on size distribution of aerosolized TiO_2, Tween-20 (Polyoxyethylene (2) Sorbitan Monolaurate) was added in different concentrations to a 6mM TiO_2 suspension. A stock solution with 2.0mM Tween-20 was prepared to facilitate dispensing of the surfactant as it was very viscous in its original form. Critical Micelle Concentration for a surfactant is the concentration above which micelles are spontaneously formed. Four different concentration of Tween 20, close to the Critical Micelle Concentration, 0.042mM (Patist et al. 2000), were added to 6mM TiO_2.

3.4 Results and Conclusions

Figure 20 shows a graph of the size distributions for 5 different concentrations of TiO_2 suspensions. The peaks that can be seen in the lower end of the size spectrum correspond to particles between the range of approximately 10nm to 80nm. These are the residual particles from impurities in water and unevaporated water droplets and possibly TiO_2 nanoparticles. Peaks corresponding to the larger diameters (approximately 200nm) represent the TiO_2 particles. This was deduced by running the nebulizer only with DI water and measuring its size distribution. The size distribution observed had a mode diameter of approximately 30nm. No secondary peak was observed for DI water. Along

with this, the concentration of larger particles increases as the TiO_2 in suspension increases, indicating a correspondence between TiO_2 particles and the peak corresponding to the larger particles.

The unformed peaks for 0.5mM and 1mM indicate low concentration of TiO_2 particles. The graph is further skewed by the presence of residual particles. It can also be observed that concentration of residual particles increases as the number of TiO_2 particles in suspension decrease. This can be explained by the larger number of empty droplets for lower concentrations. Lower TiO_2 particles result in more empty droplets which upon evaporation lead to residual particles. The contribution of unevaporated DI water droplets to residual droplets had been confirmed and will be discussed in the next section.

The mode diameters of 3mM, 6mM, and 9mM were found to be 197.5nm, 200.0nm and 195.2nm respectively. The mode diameter corresponds to the average of 5 trials with the same suspension concentration. Thus, there is not much change in the size mode diameter in this concentration range studied.

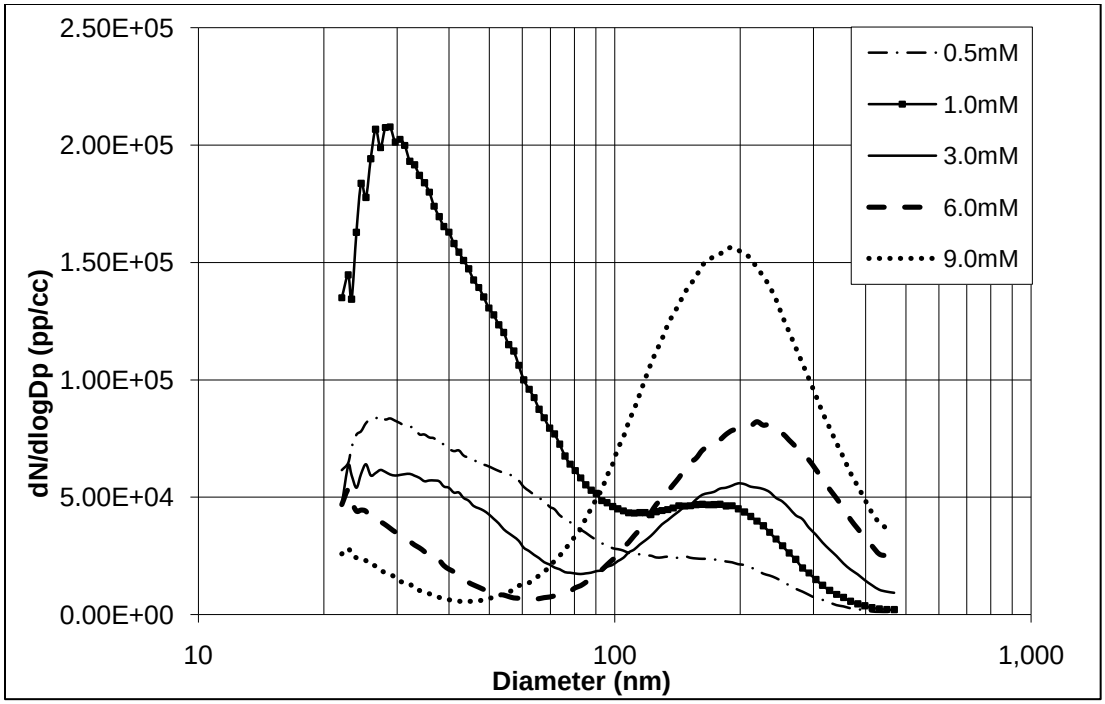

Figure 20: Particle size distribution of various concentrations of Titanium dioxide suspensions

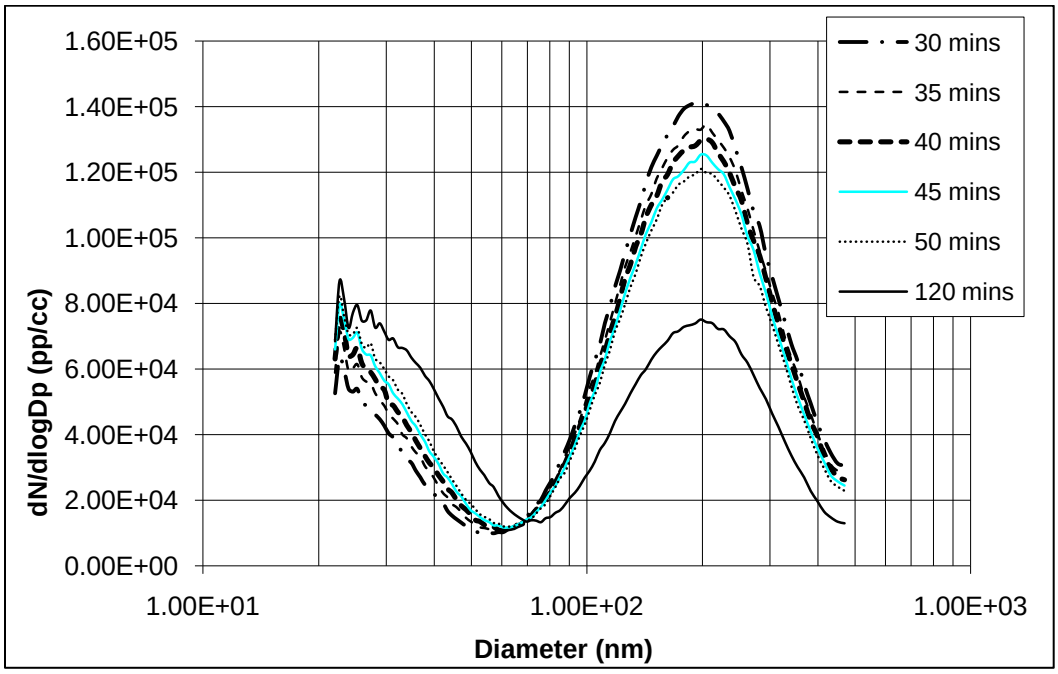

Figure 21: Size distribution of 9.0mM Titanium dioxide suspension for 6 trials taken at different times during Collison nebulizer run

Figure 21 shows the size distributions for 6.0mM TiO_2 aerosol generated by a Collison nebulizer at different times during its run. It can be seen that with time the particle concentration decreases. Along with this, the concentration of residual particles at the lower end of size spectrum also increases. This can be explained by the increase in empty droplets generated by the nebulizer, as mentioned previously. Size distributions for all concentrations of suspension followed similar patterns. One of the explanations of decreasing concentration of TiO_2 particles could be the aggregation of particles in the suspension. The results from DLS measurements are mentioned in the following paragraphs which prove that this was in fact the reason for lowering of TiO_2 concentration with time.

To confirm aggregation of particles as the cause of lowered concentration of TiO_2 particles with time, particle size distribution in the suspension was determined using DLS. Measurement of 1mM freshly prepared sample indicated agglomeration which made it difficult to get meaningful results of its size distribution. To deagglomerate the particles techniques such as bath sonication, centrifugation and probe sonication were used. Only 5 minutes of probe sonication was successful in deagglomerating the particle to make them suitable for DLS measurement. The size distribution of probe sonicated suspension can be seen in Figure 22.

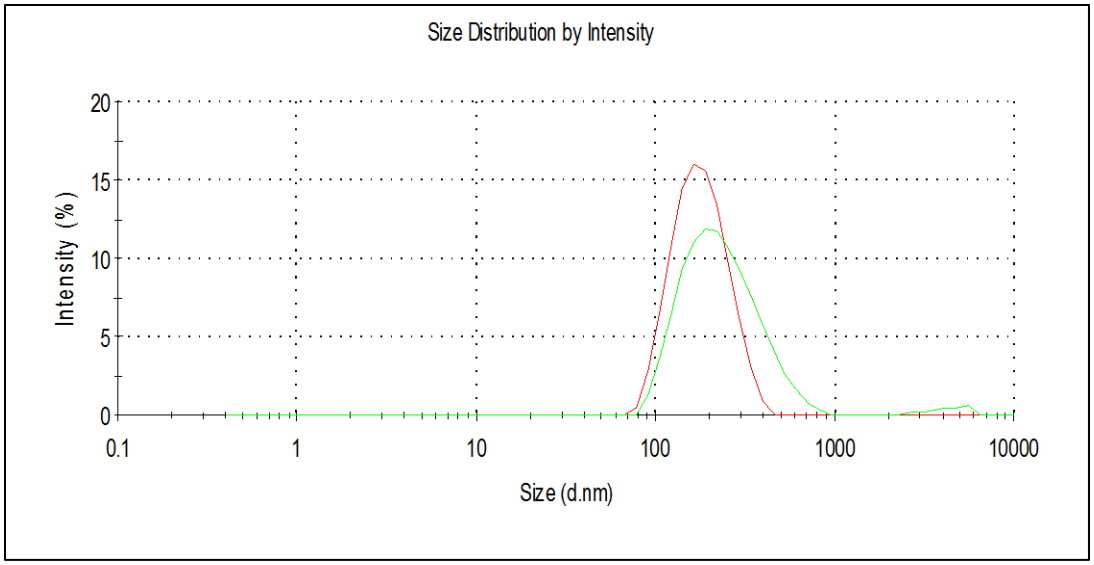

Figure 22: Size distribution measurement of 1mM Titanium dioxide suspension found using Dynamic Light Scattering (DLS) technique

The two curves in Figure 22 represents the size distribution of TiO_2 in suspension. The more monodisperse curve (red) shows the size distribution during the experiment and indicates the mode diameter to be approximately 170nm. The curve to the right (green) represents a trend in the suspension observed during the experiment. It indicates that particles were agglomerating even during the short time of experiment. Similar trends were also observed during size distribution measurements of nebulized TiO_2 particles for 3mM, 6mM and 9mM suspensions. The agglomeration can be observed in Figure 23 by the shift of mode diameter from 168nm to 191nm in 25mins.

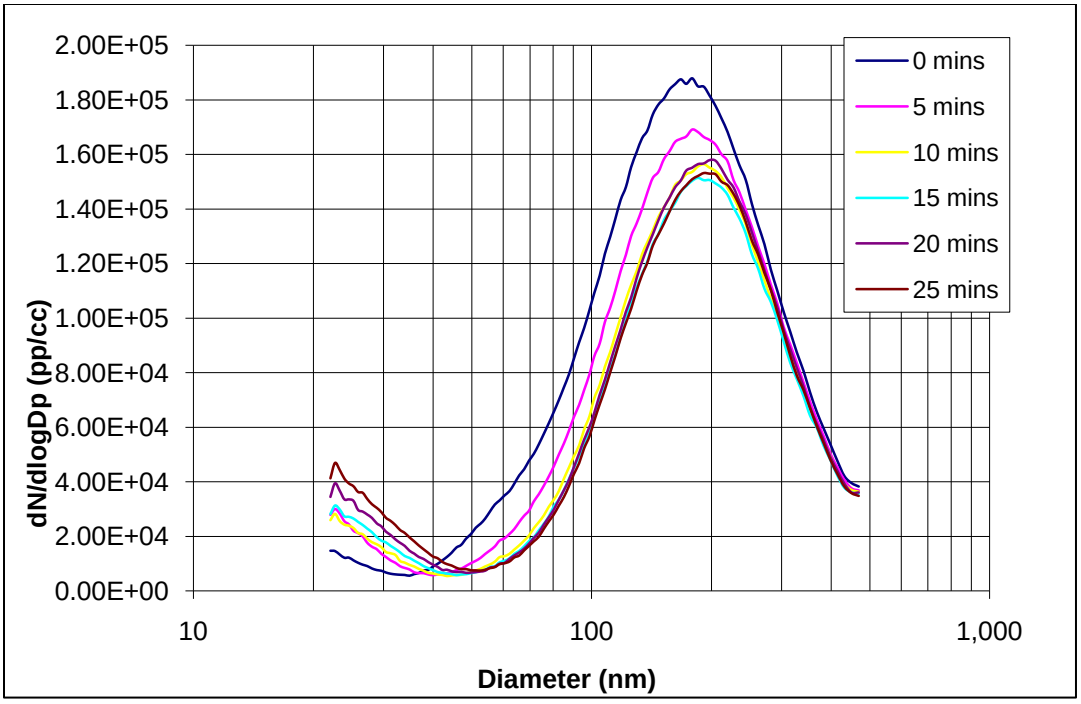

Figure 23: Agglomeration observed between size distribution measurements of 9.0mM Titanium dioxide suspension during nebulization by an increase in mode diameter for consecutive measurements

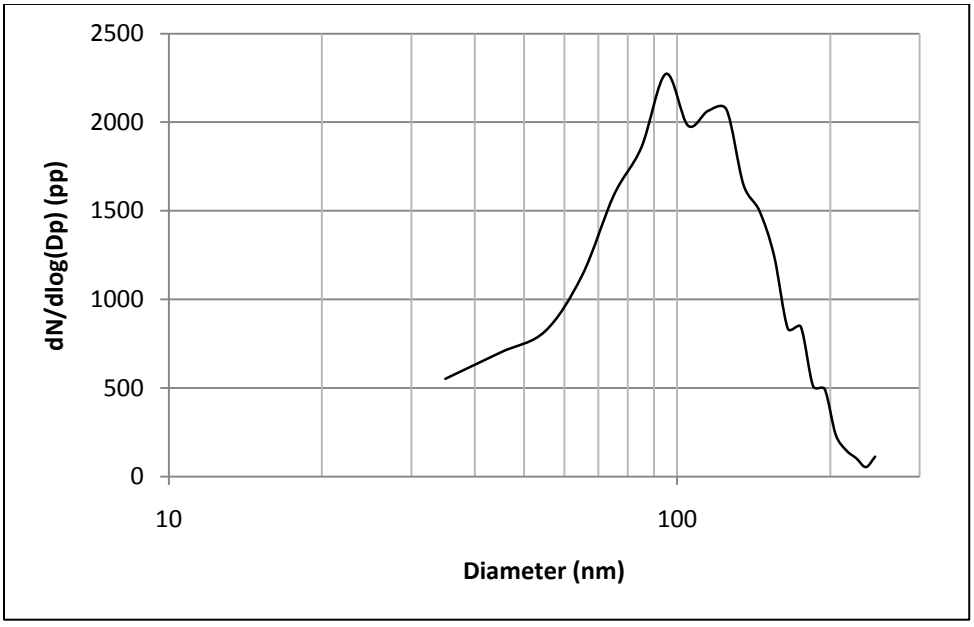

Figure 24: Size distribution of single particles in flame synthesized Titanium dioxide powder found by TEM analysis

Figure 24 shows the size distribution of flame synthesized TiO_2 particles from TEM analysis. Over 1000 particles were measured in the population, and the mode was found to be approximately 95nm. This is a relatively smaller size comparative to the particles generated by Collison nebulizer, suggesting agglomeration. The addition of different concentrations of Tween-20 to 6mM TiO_2 is shown in Figure 25.

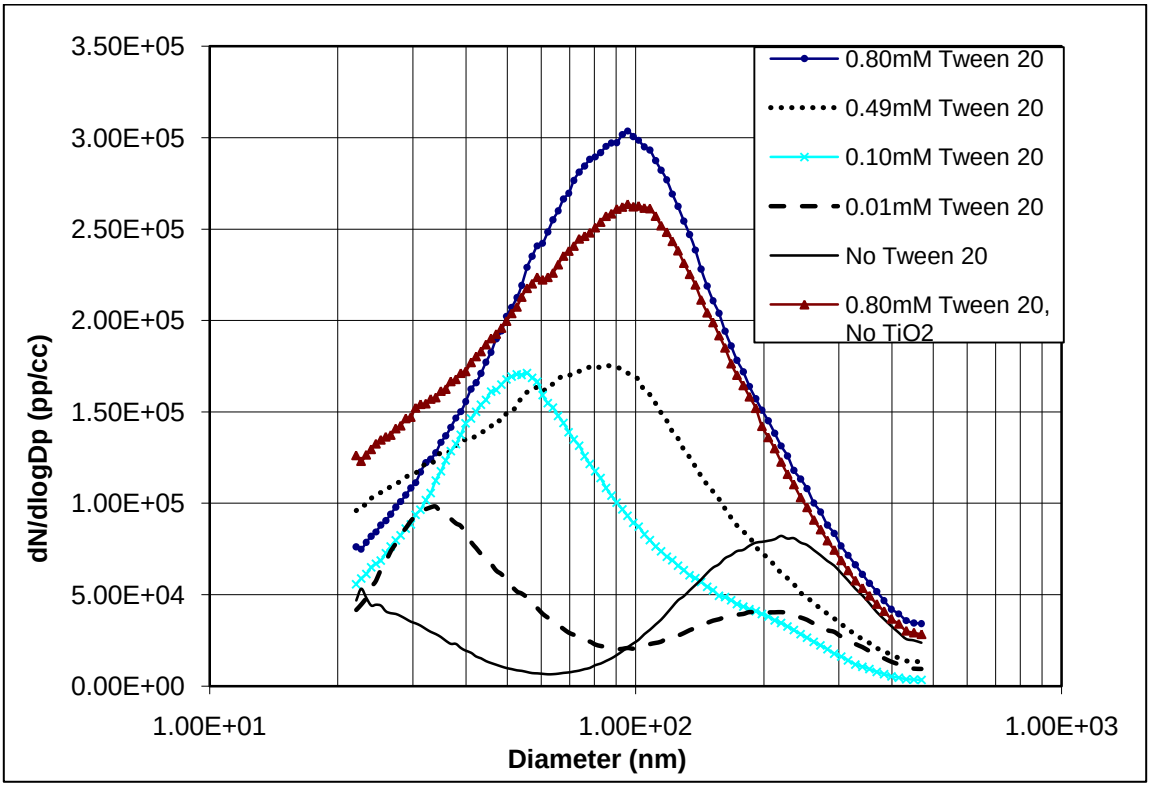

Figure 25: Size distribution of nebulized 6.0mM TiO_2 + Tween-20 suspension with varying concentrations of Tween 20

It can be seen from Figure 25 that as the concentration of surfactant decreases, the particles diameter corresponding to highest number concentration also decreases. All concentrations were chosen such that they were close to the Critical Micelle

Concentration which was 0.042mM. A trend can be observed in size distribution of TiO_2+Tween 20 aerosol. Decreasing concentration of Tween 20 in the suspension results in smaller diameter mode particles. Table 3 shows the diameter of particles at which the highest number concentrations are observed in the size distributions of aerosols with varying concentrations of Tween 20. This can be explained by the decrease in concentration of Tween 20 in the bulk suspension. Each droplet formed would have a concentration of surfactant proportional to that in the bulk suspension. As the droplets dry, the surfactant is precipitated and a particle is formed. Higher concentrations of Tween 20 in the droplets result in bigger particles present in the aerosol and hence a larger mode diameter.

Table 3: Mode diameters of particle size distribution of TiO_2 suspension with varying concentrations of Tween 20

TiO2 conc. (mM)	Tween 20 Conc. (mM)	Size Dist. Mode Diameter (nm)
6.00	0.80	96
6.00	0.49	88
6.00	0.10	56
6.00	0.01	34nm surfactant mode+212nm TiO2 peak visible

It can be observed from Figure 25, that at Tween 20 concentration of 0.01mM, two peaks are observed. It can be deduced from earlier observations of size distribution measurement of aerosol with no surfactant that the larger peak with a mode diameter 212nm belongs to the TiO_2 particles. This is because 6.0mM TiO_2 suspension had a peak at approximately 200nm. The slight increase in mode diameter with the addition of surfactant is due to the presence of an additional layer of Tween 20 over the particle surface. From this observation, it can be concluded that the surfactant does not have significant effect in emulating single particle distribution observed in powder. A possible explanation for this is the formation of agglomerates during storage of TiO_2 powder. Hard agglomerates, which can be formed due to fusion or interparticle bonds, cannot be broken by mild forces such as sonication applied during suspension preparation (Schmoll et al. 2009).

4. STUDY OF BACKGROUND PARTICLES IN AEROSOLIZED DE-IONIZED WATER

4.1 Background

As seen in Section 2.2, for calibrating the SEMS system, a solution of 99nm/204nm diameter Polystyrene Latex (PSL) particles was made in DI water. It was observed that certain background particles were present which skewed the size distribution results of PSL particles. The source of these background particles was determined to be either compressed air fed into the nebulizer, or the DI water. Analysis of compressed air determined low concentration of particles with a mode slightly above a 100nm. Thus, DI water was confirmed to be the source of particles.

Nebulization is a widespread method of converting suspension or solutions to aerosols. This technique is used in toxicology inhalation studies frequently, especially for studying the characteristics of nanoparticles. Although DI water is often used as a solvent in the nebulization process, residual particles are observed which interfere with the study of particles of concern. Studies have linked the source of these particles to be dissolved impurities inherent to water, as well as leaching from the container walls. Furthermore, the chemical composition is not yet known and may be highly variable (LaFranchi et al. 2003).

Knowledge of particles in DI water can help identify ways for removal of particles and thus make DI water better suited for applications requiring high level of

purity. The main objective of the following work was to determine the chemical composition of particles observed in DI water.

4.2 Hypothesis/Model

It was hypothesized that the residual particles observed in the calibration process were a combination of dissolved impurities in DI water and unevaporated water droplets.

The presence of water droplets in residual particles can be confirmed by changing humidity conditions in the drying tank. The lifetime of a droplet of a pure liquid is affected by the amount of moisture in the surrounding air. This is because the rate of diffusion of molecules from the surface of the droplet decreases as the moisture content of surrounding air increases. This leads to a longer drying time for the droplet. This model can also be applied to a droplet containing dissolved, non-volatile impurities. This is because the droplet initially acts like a pure liquid droplet until the concentration of impurities increases and forms a rigid crust (Charlesworth and Marshall 1960).

In this study, it was hypothesized that humidity would have an effect on the concentration of residual particles if they were unevaporated water droplets. If the residual particles were assumed to be only composed of solid impurity particles from DI water, then a change in humidity would not affect the concentration or size distribution of particles. If the particles are instead due to unevaporated water droplets, an increase in humidity would lead to lower evaporation rates and hence a higher concentration of larger residual particles.

4.3 Experimental

To determine whether water droplets contributed to the residual particles, the size distribution of aerosol generated by nebulizing DI water was measured. The measurements were made for 96% humidity and 38% humidity. The size distributions were then compared to see if a difference existed between the particle diameters or concentration of particles between the two conditions.

The experimental setup for aerosolizing DI water and measuring its size distribution at different humidity conditions is shown in Figure 26. Filtered compressed air was split into two streams. The first stream acted as input to the nebulizer and helped nebulize DI water. The other stream supplies dehumidified dilution air whose flow rate was controlled by a needle valve as shown in the setup below. A humidity meter at the top of the evaporation cylinder monitored the humidity which was controlled by adjusting the dilution air flow. The nebulizer flow rate was maintained at 2LPM whereas the dilution air was adjusted to provide the required humidity.

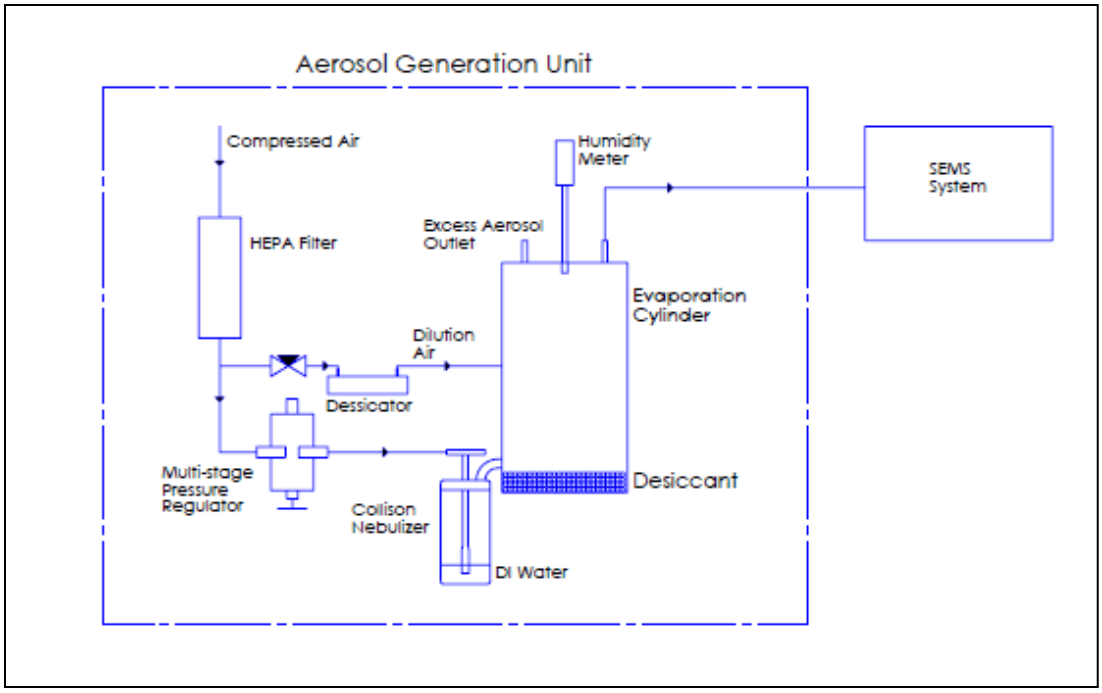

Figure 26: Experimental setup for measuring size distribution of DI water particles at different humidity conditions

Three experiments were performed for this study. In the first experiment, no dilution air was provided and the evaporation cylinder was allowed to reach stable condition. The relative humidity was thus observed to be approximately 96%. After this stable condition was reached, a size distribution measurement was taken. In the second experiment, the flow rate of dilution air was set to 4LPM which maintained a relative humidity of 38% for exiting aerosol. To confirm that the particles resulted from nebulization of DI water, the size distribution of particles in filtered air was measured. This was done by removing DI water from the nebulizer jar and measuring the size distribution of filtered air.

In the second part of the study, TEM analysis of particles collected using an Electrostatic Precipitator was conducted. A diagram for the experimental apparatus for collecting de-ionized water particles is shown in Figure 27. DI water was filled into the nebulizer jar so that about 3/8" of the nozzle was below its surface.

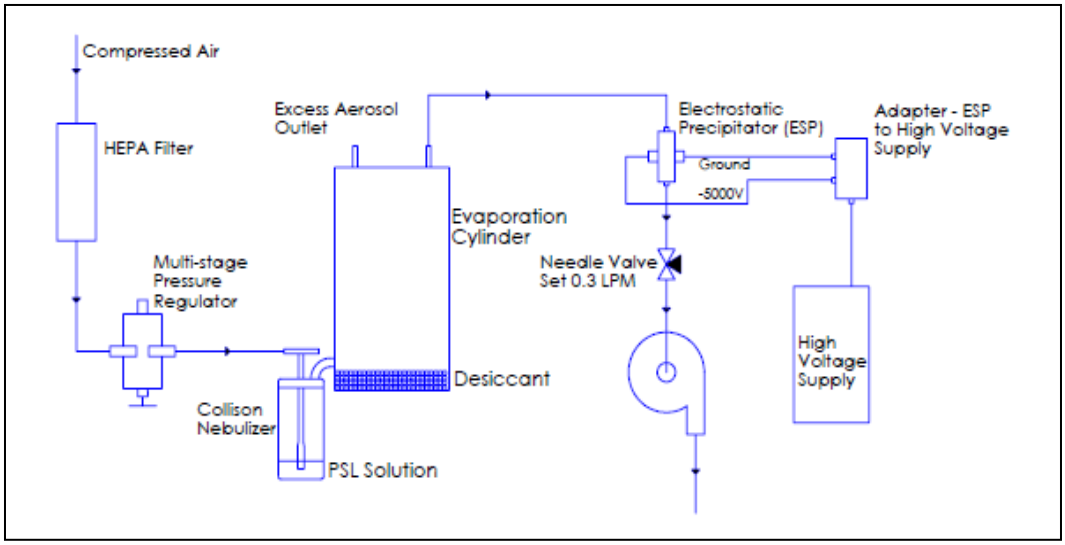

Figure 27: Schematic of apparatus setup for collection of particles in de-ionized water

Two outlets were present at the top of the cylinder. One of the outlets was open to the atmosphere and the aerosol flowed out through it at 1.70 LPM. The other outlet was connected to a pump and a flow of 0.3LPM was maintained using a needle valve upstream of the pump.

The aerosol passed through an Electrostatic Precipitator (ESP) in which de-ionized water particles were collected upon a TEM grid. A voltage of -5000V was applied on the high voltage terminal of the ESP while the other was connected to

ground. A corona discharge inside the ESP lead to collection of DI water particles on the TEM grid which was later analyzed to determine the particle composition. A number of samples were collected on the TEM grids for varying times, as it was difficult to determine how much time it would take to collect enough particles for a detailed analysis of size and chemical composition. Time periods included sampling for 1, 2, 3, 5, 20, and 60 minutes.

4.4 Results and Conclusions

Figure 28 shows the size distribution of residual particles for different humidity conditions. A peak with approximately 37nm mode diameter was observed for the 96% humidity condition. On the other hand, no such peak is observed for the size distribution of particles for 38% humidity condition. This means that unevaporated water droplets contribute to larger particles in the case where evaporation cylinder has a high humidity. In the case of low humidity more droplets are able to evaporate and hence lower concentration of residual particles. From the graph of filtered air used for dilution and nebulization, it can be concluded that the residual particles observed are not from this source.

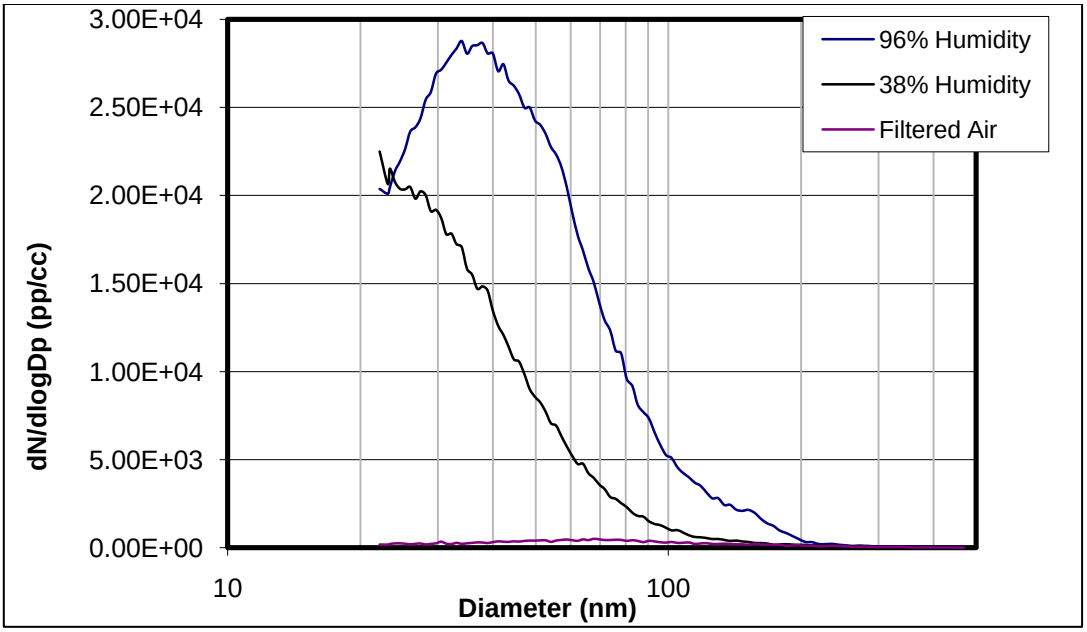

Figure 28: Particle size distribution of residual particles at different humidity conditions

Although a number of attempts were made to collect residual particles for several time periods, it was observed that a significant number of particles did not collect on the TEM grids. The TEM image of the few particles that were able to be collected is shown in Figure 29.

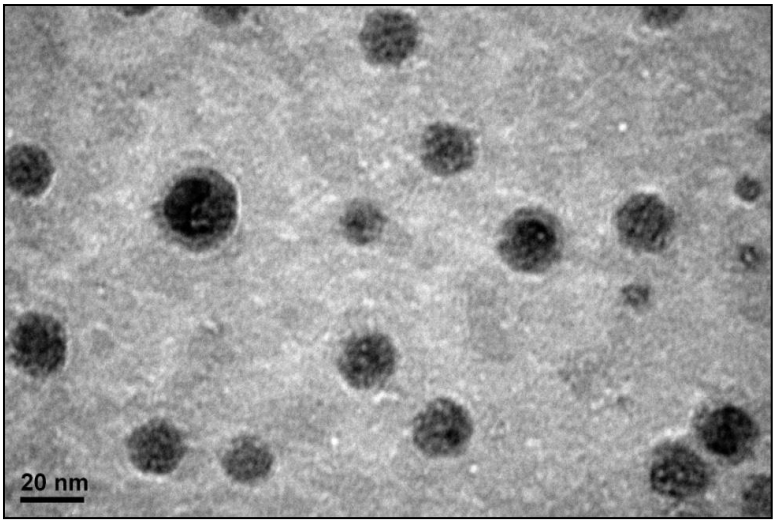

Figure 29: TEM image of residual particles in DI water collected using an Electrostatic Precipitator

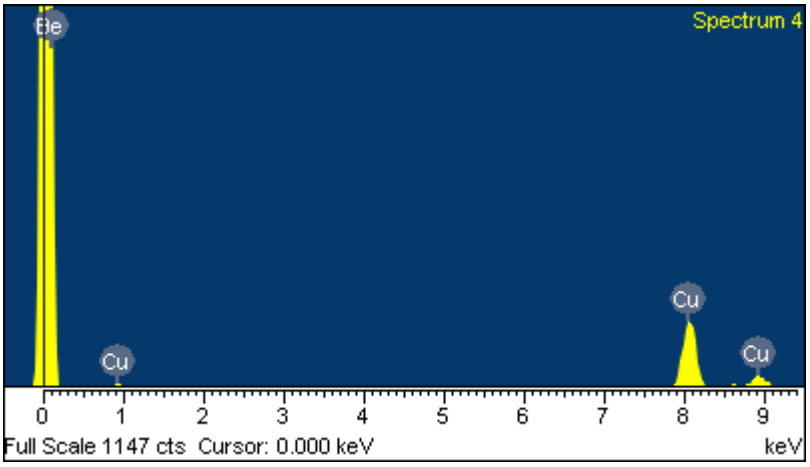

Figure 30: Quantitative analysis of DI water particles with EDS technique

Quantification through EDS analysis revealed only the presence of Copper from the TEM grid as the element present as shown in Figure 30. Possible reasons for inability of EDS to determine the composition of particles might include its small size or a possibility that the elements in the particles were low weight in which case EDS

technique is not very accurate. It can be concluded from this study that residual particles observed during the aerosolization of suspensions of DI water were composed of impurities present in DI water and unevaporated droplets of DI water. Although it was possible to observe solid residual particles from aerosolization of DI water, EDS was not able to determine the chemical composition of these particles.

5. SUMMARY

A Scanning Mobility Particle Spectrometer was designed using a Condensation Particle Counter and a Differential Mobility Analyzer to measure the particle size distribution of nanoparticles in an aerosol. It was built by accomplishing designs for hardware, which consisted of the Electrical System and the Fluid Flow System, and the software. Calibration of SEMS showed close similarity in the results of mode diameters obtained from TEM analysis and SEMS. The mode diameter of 99nm nominal diameter PSL particles was found to be 92.5 nm from TEM and 95.8nm from SEMS, a percentage difference of 3.6%. Similarly, the mode diameter for 204nm was found to be 194.9nm and 191.0nm from TEM and SEMS, respectively, a difference of 2.0%.

The SEMS was applied in the study of generation of TiO_2 particles from Collison nebulizer and residual particles in the aerosolization of de-ionized water. The Collison nebulizer generated TiO_2 particles with a mode diameter of 197.5nm, 200nm, and 195.2nm, respectively, for 3mM, 6mM and 9mM of TiO_2 suspension which was higher as compared to 95.0nm for the powder using TEM analysis. SEMS measurements indicated a decreasing concentration of particles generated by the Collison nebulizer with time and Dynamic Light Scattering technique confirmed agglomeration in the suspension as the primary reason for increased mode diameter and decreasing concentration of TiO_2 aerosol. It was not possible to emulate single particle size distribution by the use of surfactant, Tween 20, which only increased the concentration of particles generated during the nebulizer run. Finally, by studying residual particles in

DI water, observed during the SEMS calibration process, it was found that the residual particles are a mixture of solid impurity particles and unevaporated liquid droplets.

REFERENCES

Aitken, J. (1890). On a Simple Pocket Dust Counter, *Proceedings of Royal Society of Edinburgh*, 39-54.

Baron, P. A. and Willeke, K. (2001). *Aerosol Measurement: Principles, Techniques, and Applications*. Wiley, New York.

Charlesworth, D. H. and Marshall, W. R. (1960). Evaporation from Drops Containing Dissolved Solids. *Aiche J* 6:9-23.

Colvin, V. L. (2003). The Potential Environmental Impact of Engineered Nanomaterials. *Nature Biotechnology* 21:1166-1170.

Erikson, H. A. (1921). Change of Mobility of the Positive Ions in Air with Age. *Physics Review* 18:100-101.

Flagan, R. C. (1998). History of Electrical Aerosol Measurements. *Aerosol Science and Technology* 28:301-380.

Fuchs, N. A. (1963). On the Stationary Charge Distribution on Aerosol Particles in Bipolar Ionic Atmosphere. *Pure and Applied Geophysics* 56:185-193.

Hinds, W. C. (1999). *Aerosol Technology : Properties, Behavior, and Measurement of Airborne Particles*. Wiley, New York.

Hood, E. (2004). Nanotechnology: Looking as We Leap. *Environmental Health Perspectives* 112:A740-A749.

Knutson, E. O. and Whitby, K. T. (1975). Aerosol Classification by Electric Mobility: Apparatus, Theory and Applications. *Aerosol Science and Technology* 6:443-451.

LaFranchi, B. W., Knight, M. and Petrucci, G. A. (2003). Leaching as a Source of Residual Particles from Nebulization of Deionized Water. *Journal of Aerosol Science* 34:1589-1594.

Navrotsky, A. (2000). Nanomaterials in the Environment, Agriculture, and Technology (Neat). *Journal of Nanoparticle Research* 2:321-323.

Patist, A., Bhagwat, S. S., Penfield, K. W., Aikens, P. and Shah, D. O. (2000). On the Measurement of Critical Micelle Concentrations of Pure and Technical-Grade Nonionic Surfactants. *J Surfactants Deterg* 3:53-58.

Reich, D. H., Tanase, M., Hultgren, A., Bauer, L. A., Chen, C. S. and Meyer, G. J. (2003). Biological Applications of Multifunctional Magnetic Nanowires (Invited). *Journal of Applied Physics* 93:7275-7280.

Schick, M. J. (1967). *Nonionic Surfactants*. M. Dekker, New York,.

Schmoll, L. H., Elzey, S., Grassian, V. H. and O'Shaughnessy, P. T. (2009). Nanoparticle Aerosol Generation Methods from Bulk Powders for Inhalation Exposure Studies. *Nanotoxicology* 1.

Shimada, M., Wang, W. N., Okuyama, K., Myojo, T., Oyabu, T., Morimoto, Y., Tanaka, I., Endoh, S., Uchida, K., Ehara, K., Sakurai, H., Yamamoto, K. and Nakanishi, J. (2009). Development and Evaluation of an Aerosol Generation and Supplying

System for Inhalation Experiments of Manufactured Nanoparticles. *Environmental Science & Technology* 43:5529-5534.

Wang, S. C. and Flagan, R. C. (1990). Scanning Electrical Mobility Spectrometer. *Aerosol Science and Technology* 13:230-240.

Wiedensohler, A. (1988). An Approximation of the Bipolar Charge-Distribution for Particles in the Sub-Micron Size Range. *Journal of Aerosol Science* 19:387-389.

Zahn, M. (2001). Magnetic Fluid and Nanoparticle Applications to Nanotechnology. *Journal of Nanoparticle Research* 3:73-78.

Zhang, S. H., Akutsu, Y., Russell, L. M., Flagan, R. C. and Seinfeld, J. H. (1995). Radial Differential Mobility Analyzer. *Aerosol Science and Technology* 23:357-372.

Zhao, B., Yang, Z. W., Wang, J. J., Johnston, M. V. and Wang, H. (2003). Analysis of Soot Nanoparticles in a Laminar Premixed Ethylene Flame by Scanning Mobility Particle Sizer. *Aerosol Science and Technology* 37:611-620.

Zhu, Y. F., Hinds, W. C., Kim, S. and Sioutas, C. (2002). Concentration and Size Distribution of Ultrafine Particles Near a Major Highway. *J Air Waste Manage* 52:1032-1042.

APPENDIX

AVERAGE DROPLETS DRYING TIME GENERATED FROM COLLISON NEBULIZER

Values of parameters for calculation:

Gas constant, $R = 8.314 J / K - mol$

Water density, $\rho_p = 1000 kg / m^3$

Count Median Diameter (CMD) for droplets generated by Collison nebulizer, $CMD = 8.89 \times 10^{-7} m$

Geometric standard deviation, $\sigma_g = 1.8$

Diffusion coefficient for water vapor molecules in air, $D_v = 2.4 \times 10^{-5} m^2 / s$

Molecular mass of water, $M = 0.018 kg / mol$

Temperature at infinity, $T_\infty = 20^o C$

Relative humidity inside drying tank, $RH = 96.7\%$

Calculation:

Diameter of average size water droplet generated from Collison nebulizer,

$$d_p = CMD \exp\left(0.5 \times \sigma_g^2\right) = 4.49 \times 10^{-6} m \quad [1]$$

Saturation ratio inside drying tank,

$$S_R = RH / 100 = 0.967 \quad [2]$$

Temperature at droplet surface,

$$T_d = \frac{\left(6.65 + 0.345T_\infty + 0.0031T_\infty^2\right) \times \left(S_R - 1\right)}{\left(1 + \left(0.082 + 0.00782 \times T_\infty\right)^{S_R}\right)} + T_\infty = 19.6^o C \quad [3]$$

Partial pressure of vapor at droplet surface,

$$p_d = \exp\left(16.7 - \frac{4060}{\left(T_d + 273\right) - 37}\right) = 2261.47 Pa \quad [4]$$

Saturation pressure at ambient temperature,

$$p_s = \exp\left(16.7 - \frac{4060}{\left(T_\infty + 273\right) - 37}\right) = 2317.82 Pa \quad [5]$$

Partial pressure of vapor at infinity,

$$p_\infty = p_s \times T_\infty = 2241.33 Pa \quad [6]$$

Evaporation time for droplet,

$$t = \frac{R \times \rho_p \times d_p^2}{8 \times D_v \times M \times \left(\frac{p_d}{T_d} - \frac{p_\infty}{T_\infty}\right)} = 3.037 \sec \quad [7]$$

Additional Information:

1. Fuchs effect is neglected for particle diameters greater than 1μm.
2. Kelvin effect can be neglected for particles of water greater than 0.1μm.

VITA

Name:	Gagan Singh
Address:	Department of Mechanical Engineering, Texas A&M University, 3123 TAMU, College Station, TX 77843-3123, USA
Email Address:	gsingh.07@gmail.com
Education:	B.S., Mechanical Engineering, Texas A&M University, 2006 M.S., Mechanical Engineering, Texas A&M University, 2010